Evolutions of spinning bodies moving in rotating black hole spacetimes

Zoltán Keresztes^{1,†} and Balázs Mikóczi^{2,‡}

¹ Department of Theoretical Physics, University of Szeged, Tisza Lajos krt. 84-86, Szeged 6720, Hungary

² Research Institute for Particle and Nuclear Physics,

Wigner RCP H-1525 Budapest 114, P.O. Box 49, Hungary

[†] E-mail: zkeresztes@titan.physx.u-szeged.hu

[‡] E-mail: mikoczi.balazs@wigner.mta.hu

The evolutions of spinning test bodies are investigated in rotating (Kerr, Bardeen-like and Hayward-like) black hole spacetimes. Spin vector precessional equations are derived in both comoving and zero 3-momentum frames from the Mathisson-Papapetrou-Dixon (MPD) equations using either the Frenkel-Mathisson-Pirani or the Tulczyjew-Dixon spin supplementary condition. The comoving and the zero 3-momentum frames are set up from either the static or the zero angular momentum observer frame by instantaneous Lorentz-boosts. However when the body passes over the ergosphere only the boosted zero angular momentum frame can be used for description of the spin dynamics during the whole evolution. Far from the black hole the difference between the boosted static and zero angular momentum frames is unsignificant. Numerical applications are presented for spinning bodies moving along spherical-like, zoom-whirl (thus their existence is confirmed based on the MDP equations) and unbound orbits. The spin evolutions are presented in the boosted static and zero angular momentum observer frames and they are compared, obtaining only differences in the near black hole region. We have found the spin magnitude influences on the orbit evolution, and the spin precessional angular velocity is highly increased near and inside the ergosphere.

I. INTRODUCTION

Both the orbital and the spin dynamics of compact binary systems have a renewed interest. All observed gravitational waves originated from compact binary systems composed of black holes or neutron stars ([1–8]). In two cases the spin of the merging black holes was identified with high significance [2, 8, 9]. In addition in a binary system the dominant supermassive black hole spin precession was identified from VLBI radio data spanning over 18 years [10].

In the post-Newtonian (PN) approximation the lowest order spin contributions to the dynamics comes from the spin-orbit, spin-spin and quadrupole-monopole interactions [11–14]. The spin effects on the orbit leaded to set up generalized Kepler equations [15–18]. The analytical description of the secular spin dynamics for black holes is given in Refs. [19] and [20]. Based on the PN description several interesting spin related behaviours were identified in compact binary systems, like transitional precession [21], equilibrium configurations [22], spin-flip [23], spin flip-flop [24] and wide precession [25].

The Mathisson-Papapetrou-Dixon (MPD) equations [26–30] describe the dynamics of binaries with significantly different masses more accurately than the PN approximation in the strong gravitational field regime where the PN parameter is not small. The black hole binary systems with small mass ratio are among the most promising sources for gravitational waves in the frequency sensitivity range of the planned LISA - Laser Interferometer Space Antenna [31, 32]. In addition near the central supermassive black holes in the galaxies many stellar black holes are expected to exist [33–35].

The MPD equations are not closed, a spin supplemen-

tary condition¹ (SSC) is necessary to choose [28, 37–44] which defines the point at which the four-momentum and the spin are evaluated. A non-spinning body follows a geodesic trajectory while a spinning one does not [45, 46]. Spinning bodies governed by the MPD equations were already studied on Kerr background. Circular orbits in the equatorial plane can be unstable not only in the radial direction but also in the perpendicular direction to the equatorial plane due to the spin [47]. The spin-curvature effect strengthens with spin and with non-homogeneity of the background field [46]. The MPD equations admit many chaotic solutions, however these do not occur in the case of extreme mass ratio binary black hole systems [48–50]. Analytic studies on the deviation of the orbits from geodesics due to the presence of a small spin are presented in Refs. [51–53]. Highly relativistic circular orbits in the equatorial plane occur in much wider space region for a spinning body than for a non-spinning one [54]. Spin-flip-effects may occur when the magnetic type components of quadrupole tensor are non-negligible [55]. Corrections due to the electric type components of quadrupole tensor to the location of innermost stable circular orbit in the equatorial plane and to the associated motion's frequency were determined in Ref. [56]. An exact expression for the periastron shift of a spinning test body moving in the equatorial plane is derived [57]. The influences of the affine parameter choice on the constants of motion in different SSC were also considered [58]. Frequency domain analysis of motion and spin precession was presented in Ref. [59].

Considering geodesic trajectories, the periastron ad-

¹ Both the PN dynamics with spin-orbit coupling and the gravitational multipole moments depend on the SSC [13, 36].

vance can become such significant in the strong gravitational field regime that the test particle follows a zoom-whirl orbit [60–62]. For non-spinning particles the topology of these orbits was encoded by a rational number [63, 64]. Numerical relativity confirmed the existence of zoom-whirl orbits [65–70], and they also occur in the 3 PN dynamics with spin-orbit interaction [71, 72]. Here we will present zoom-whirl orbits occurring in the MPD dynamics for the first time. In addition these orbits pass over the ergosphere where the PN approximation fails.²

Hyperbolic orbits of spinning bodies were analytically studied in both the PN [73] and the MPD [74] dynamics. Analytic computations in Ref. [74] were carried out for small spin magnitudes when the spin is parallel to the central black hole rotation axis and the body moves in the equatorial plane. In this configuration both the spin magnitude and direction are conserved, but they have non-negligible influences on the orbit. In our numerical consideration the spin is not parallel to the black hole rotation axis. As consequences, the body's orbit is not confined to the equatorial plane and the spin direction evolves. In addition the closest approach distance is inside the ergosphere where the PN approximation cannot be used.

Our investigations are not only applied in the Kerr spacetime but also in regular black hole backgrounds. The first spacetime containing a nonrotating regular black hole was suggested by Bardeen [75]. This metric was interpreted as the spacetime surrounding a magnetic monopole occurring in a nonlinear electrodynamics [76]. Another nonrotating regular black hole was introduced by Hayward [77] having similar interpretation [78]. The spacetime family containing the Bardeen and Hayward cases was generalized for rotating black holes [79] which we will use here³.

In this paper we investigate the orbit and spin evolutions of bodies moving in Kerr, Bardeen-like and Hayward-like spacetimes and governed by the MPD equations with Frenkel-Mathisson-Pirani (FMP) and Tulczyjew-Dixon (TD) SSCs. When the covariant derivatives of the spin tensor and the four-momentum along the integral curve of the centroid determined by the SSC are small, this system reduces to a geodesic equation with parallel transported spin discussed in Ref. [83]. In this sense the present article can be considered as the generalization of Ref. [83] with non-negligible spin-curvature corrections causing that the centroid orbit is non-geodesic and the spin is not parallel transported. As Bini, Ger-

alico and Jantzen pointed out the spin dynamics can be described suitably in the comoving Cartesian-like frame obtained by boosting the Cartesian-like frame associated to the family of static observers (SOs). This is because SOs do not move with respect to the distant stars. Thus the Cartesian-like axes locked to SOs define good reference directions to which the variation of the spin vector can be compared. Here we derive the spin evolution equation in the comoving Cartesian-like frame based on the MPD system. However SO does not exist inside the ergosphere of the rotating black hole and thus its frame cannot be used for description of the dynamics when the spinning body passes over this region. Therefore the spin dynamics in a Cartesian-like frame obtained by an instantaneous Lorentz-boost from the frame associated to the zero angular momentum observer (ZAMO) is also presented, which can be used inside the ergosphere. The boosted SO and ZAMO frames relate to each other by a spatial rotation outside the ergosphere. The rotation angle between these boosted frames is unsignificant far from the rotating black hole.

In Section II the MPD equations, the spin supplementary conditions, the rotating (Kerr, Bardeen-like and Hayward-like) black hole spacetimes and the frames associated with the families of SOs and ZAMOs are introduced. In Section III the representations of spin and orbit evolutions are given. For this purpose we introduce two frames by instantaneous Lorentz boosts of SO and ZAMO frames, which comoves with an observer having an arbitrary four velocity U. The relation between the boosted frames is discussed (additional expressions are given in Appendix B). In the case of FMP SSC, U agrees with the four velocity of the moving body's centroid. When using TD SSC U means either the centroid or the zero 3-momentum observer four velocity. The spin evolution equations are derived in these U-frames. First the spin precession is described with respect to the boosted spherical coordinate triad associated with either the SOs or ZAMOs. Then we introduce Cartesian-like triads in the rest spaces of SOs and ZAMOs. The spin precession with respect to the corresponding boosted Cartesian-like frames is also derived. The relations between the spin angular velocities in the boosted SO and ZAMO frames are discussed. In addition for characterizing the orientation of the instantaneous plane of the motion a kinematical quantity is introduced. In Section IV we apply the derived spin equations for numeric investigations when the body moves along spherical-like, zoom-whirl and unbound orbits. Section V contains the concluding remarks.

We use the signature -+++, and units where c=G=1, with speed of light c and gravitational constant G. The bold small Greek indices take values 1, 2 and 3, while the bold capital and the small Latin indices 0, 1, 2 and 3. In addition, the following small bold Latin indices \mathbf{i} , \mathbf{j} , \mathbf{k} , \mathbf{m} take values from $\{\mathbf{x}, \mathbf{y}, \mathbf{z}\}$. Finally, the bold indices are frame indices, while the non-bold indices are spacetime coordinate indices.

 $^{^2}$ At the ergosphere the value of the PN expansion parameter is typically about 1/2.

³ There are discussions (see Refs. [80–82]) on that the rotating regular black hole spacetimes given in Ref. [79] are not exact solutions of the field equations. However the spacetime family given analytically differs only perturbatively from the exact solution [82], therefore it is suitable for consideration of spinning bodies evolutions.

II. EQUATIONS OF MOTION FOR SPINNING BODIES IN ROTATING BLACK HOLE SPACETIMES

A. MPD equations and SSCs

In the pole-dipole approximation the motion of an extended spinning body in curved spacetime is governed by the Mathisson-Papapetrou-Dixon (MPD) equations [26–30] which read as

$$\frac{Dp^a}{d\tau} \equiv u^c \nabla_c p^a = F^a \,\,, \tag{1}$$

$$\frac{DS^{ab}}{d\tau} \equiv u^c \nabla_c S^{ab} = p^a u^b - u^a p^b , \qquad (2)$$

with

$$F^{a} = -\frac{1}{2} R^{a}_{bcd} u^{b} S^{cd} . {3}$$

Here ∇_c is the covariant derivative, p^a and S^{ab} are the four-momentum and the spin tensor of the moving body, respectively, and R^a_{bcd} is the Riemann tensor. Finally $u^a = dx^a/d\tau$ is the four-velocity of the representative point for the extended body at spacetime coordinate $x^a(\tau)$ with an affine parameter τ .

Choosing the affine parameter τ as the proper time: $u^a u_a = -1$, Eq. (2) can be written as

$$p^a = mu^a - u_b \frac{DS^{ab}}{d\tau} , \qquad (4)$$

where $m = -u_a p^a$ is the mass in the rest frame of the observer moving with velocity u^a . Equation (4) shows that the momentum p^a and the kinematic four velocity u^a are not proportional to each other for a spinning body in general.

In order to close the MPD equations an SSC is necessary to choose which defines the representative point of the extended body. There are some proposed SSC, namely the Frenkel-Mathisson-Pirani [26, 37, 38], the Newton-Wigner-Pryce, [40, 41] the Corinaldesi-Papapetrou, [27, 39] and the Tulczyjew-Dixon [28, 42]. In the following we will apply the Frenkel-Mathisson-Pirani and the Tulczyjew-Dixon SSCs. The representative point of the extended body is referred as the center of mass or the centroid.

We note that if the covariant derivatives of the spin tensor and the four-momentum along the integral curve of u^a are small, i.e. the right hand sides of Eqs. (1) and (2) are negligible, p^a becomes proportional to u^a which satisfies the geodesic equation because m is a constant. Then introducing a spin four-vector perpendicular to u^a (see Eq. (2.5) of Ref. [84]), it will be parallel transported along the trajectory. The geodesic equations with parallel transported spin vector was investigated in Ref. [83].

1. Equations of motion with Frenkel-Mathisson-Pirani SSC

The FMP SSC imposes

$$u_a S^{ab} = 0 . (5)$$

This SSC yields two constants of motion (see Ref. [46]) since

$$\frac{D}{d\tau} \left(S_{ab} S^{ab} \right) = 0 , \quad \frac{dm}{d\tau} = 0 . \tag{6}$$

This SSC reduces the independent components of the spin tensor to three, therefore it is worth to introduce a spin vector being perpendicular to u^a as

$$s^a = -\frac{1}{2}\eta^{abcd}u_b S_{cd} , \qquad (7)$$

with 4-dimensional Levi-Civita tensor η_{abcd} which is totally antisymmetric and $\eta_{0123} = \sqrt{-g}$, where g is the determinant of the metric. The inverse expression of (7) is

$$S^{ab} = \eta^{ab}_{cd} u^c s^d . (8)$$

The magnitude of s^a is a constant of motion since

$$s_a s^a = \frac{1}{2} S_{cd} S^{cd} . (9)$$

The relation (4) can be written as

$$p^a = mu^a + S^{ab}a_b (10)$$

with acceleration $a^a \equiv Du^a/d\tau$. Now taking into account $s_a S^{ab} = 0$, we find that $s_a p^a = 0$.

The covariant derivative of s^a along the worldline of the centre of mass is

$$\frac{Ds^a}{d\tau} = u^a a_b s^b \ . \tag{11}$$

This tells us that the spin vector is Fermi-Walker transported along the worldline of the centroid which makes the FMP SSC preferred from mathematical point of view [85–87]. For negligible acceleration a^a , the centroid follows a geodesic curve along which s^a is parallel transported.

In addition the FMP SSC together with the MPD equations yields a unique formula for the derivative of u^b along the worldline of the centroid [44] as

$$a^a = \frac{1}{s^c s_c} \left(\frac{s^b F_b}{m} s^a - p_b S^{ab} \right) . \tag{12}$$

This and Eq. (10) result in the following velocity-momentum relation realized recently in Ref. [88]:

$$mu^a = p^a + \frac{2S^{ab}S_{bc}p^c}{S^{de}S_{de}}$$
 (13)

Thus the initial data set $\{x^a, p^a, S^{ab}\}|_{\tau_{in}}$ provides a unique solution of the MPD equation with FMP SSC. Taking the derivative of (13) and using the FMP SSC we find (12). However we must mention that (13) does not automatically ensure that $u_aS^{ab}=0$ for arbitrary p^a and S^{ab} . In order to ensure this, we have a constraint between the four momentum and the spin tensor emerging from the contraction of Eq. (13) with S_{ab} .

In addition the data set $\{x^a, p^a, S^{ab}\}|_{\tau_{in}}$ cannot be inverted for the set $\{x^a, m, u^a, S^{ab}\}|_{\tau_{in}}$ due to Eq. (10). One needs the data set $\{x^a, m, u^a, S^{ab}, a^a\}|_{\tau_{in}}$ to fix the trajectory. For a set $\{x^a, m, u^a, S^{ab}, a^a\}|_{\tau_{in}}$ we can obtain a non-helical and infinite number of helical trajectories for different a^a . In principle all worldlines where the conditions $u_a u^a = -1$, $u_a S^a = 0$ and $p_a S^a = 0$ are satisfied can be used for representation of the moving body [86].

2. Equations of motion with Tulczyjew-Dixon SSC

The TD SSC imposes

$$p_a S^{ab} = 0. (14)$$

This SSC also yields two constants of motion (see Ref. [46]):

$$\frac{D}{d\tau} \left(S_{ab} S^{ab} \right) = 0 \; , \; \frac{dM}{d\tau} = 0 \; , \tag{15}$$

where $M = \sqrt{-p^a p_a}$ is the dynamical mass. In addition the TD SSC together with the MPD equations results in the following velocity-momentum relation [46, 89, 90]:

$$u^{b} = \frac{m}{M^{2}} \left(p^{b} + \frac{2S^{ba}R_{aecd}p^{e}S^{cd}}{4M^{2} + R_{aecd}S^{ae}S^{cd}} \right) . \tag{16}$$

Then the normalization $u^b u_b = -1$ gives a relation $m^2 = m^2 (p^a, S^{bc})$. The inverse relation of (16) was obtained in Ref. [88]:

$$p^{a} = \frac{M^{2}}{m} \left(u^{a} - \frac{1}{2M^{2}} R_{bcde} u^{c} S^{de} S^{ab} \right) , \qquad (17)$$

with

$$M^2 = m^2 - \frac{1}{2} S^{ab} u_a R_{bcde} u^c S^{de} . {18}$$

Thus both $\{x^a, p^a, S^{ab}\}|_{\tau_{in}}$ and $\{x^a, m, u^a, S^{ab}\}|_{\tau_{in}}$ initial data sets provide a unique solution of the MPD equations with TD SSC.

The spin vector which is perpendicular to p^a is introduced as

$$S^a = -\frac{1}{2M} \eta^{abcd} p_b S_{cd} , \qquad (19)$$

with inverse relation

$$S^{ab} = \frac{1}{M} \eta^{ab}_{cd} p^c S^d . \tag{20}$$

The magnitude of this spin vector is a constant of motion, because

$$S_a S^a = \frac{1}{2} S_{cd} S^{cd} . (21)$$

Since

$$S_a S^{ab} = 0 = S_a p^a \ , \tag{22}$$

the contraction of Eq. (16) with S_b results in $S_b u^b = 0$. Finally, the covariant derivative of S^a along the worldline of the centroid is

$$\frac{DS^a}{d\tau} = \frac{S^b F_b}{M^2} p^a \ . \tag{23}$$

If F^a is negligible, S^a is parallel transported along the worldline of the centroid. In addition then the centroid moves along a geodesic curve which can be shown from the MPD equations together with (4) and (23).

B. Rotating black hole spacetimes

The line element squared describing the considered rotating black hole spacetimes in Boyer-Lindquist coordinates reads as [79, 91]

$$ds^{2} = -\frac{\Delta - a^{2} \sin^{2} \theta}{\Sigma} dt^{2} - \frac{2a\mathcal{B} \sin^{2} \theta}{\Sigma} dt d\phi + \frac{\Sigma}{\Lambda} dr^{2} + \Sigma d\theta^{2} + \frac{\mathcal{A}}{\Sigma} \sin^{2} \theta d\phi^{2} , \qquad (24)$$

with

$$\Sigma = r^2 + a^2 \cos^2 \theta$$
, $\Delta = r^2 + a^2 - 2[\mu + \alpha(r)]r$,

$$\mathcal{B} = r^2 + a^2 - \Delta$$
, $\mathcal{A} = (r^2 + a^2)^2 - \Delta a^2 \sin^2 \theta$. (25)

In the Kerr spacetime $\alpha(r)$ vanishes and μ and a denote the mass and rotation parameters, respectively. The function $\alpha(r)$ occurs when a non-linear electromagnetic field is present. It is given by

$$\alpha\left(r\right) = \frac{\mu_{em}r^{\gamma}}{\left(r^{\nu} + q_{m}^{\nu}\right)^{\gamma/\nu}},\qquad(26)$$

where

$$\mu_{em} = \frac{q_m^3}{\sigma} \tag{27}$$

is the electromagnetically induced ADM mass. Here σ controls the strength of nonlinear electrodynamic field and carries the dimension of length squared, q_m is related to the magnetic charge (see Ref. [78]) and the powers are $(\gamma=3,\nu=2)$ for the Bardeen-like and $(\gamma=3,\nu=3)$ for the Hayward-like spacetimes.

The stationary limit surfaces and the event horizon (if they exist) are determined by the solutions of Eqs.

$$g_{tt} = 0 \iff \Delta - a^2 \sin^2 \theta = 0 , \qquad (28)$$

and

$$g^{rr} = 0 \iff \Delta = 0 , \qquad (29)$$

respectively. The structure of the spacetime depends on the number of real, positive solutions of Eqs. (28) and (29). For the Kerr spacetime $\mu_{em}=0$, then the location of stationary limit surfaces and event horizons are given by

$$\frac{r_{S\pm}}{\mu} = 1 \pm \sqrt{1 - \frac{a^2}{\mu^2} \cos^2 \theta} , \qquad (30)$$

$$\frac{r_{H\pm}}{\mu} = 1 \pm \sqrt{1 - \frac{a^2}{\mu^2}},\tag{31}$$

respectively. For $a/\mu < 1$ there are two stationary limit surfaces and event horizons. The region which is located outside the outer event horizon but inside the outer stationary limit surface is called ergosphere. The spacetime is free from the singularity for $\mu = 0$ and $\gamma \geq 3$. The first and the second panels of Fig. 3 in Ref. [79] indicates the region in the parameter space of a and $q = q_m/\mu_{em}$ for the Bardeen and the Hayward subcases, respectively, where the above line element squared describes a regular black hole.

In the spacetimes having symmetries, constants of motion associated to each Killing vector ξ^a (which obeys the Killing equation $\nabla_{(a}\xi_{b)}=0$) emerge [29] as

$$C_{\xi} = \xi^a p_a + \frac{1}{2} S^{ab} \nabla_a \xi_b . \tag{32}$$

Since the rotating black hole spacetimes have a timelike ∂_t and a spatial ∂_{ϕ} Killing vectors due to the staticity and axial symmetry, there are two constants of motion [48]:

$$E = -p_t - \frac{1}{2} S^{ab} \partial_a g_{bt} ,$$

$$J_z = p_\phi + \frac{1}{2} S^{ab} \partial_a g_{b\phi} .$$
(33)

At spatial infinity E means the energy of the spinning body and J_z is the projection of the total momentum to the symmetry axis. These constants are used for checking the numerical accuracy.

1. Static and zero angular momentum observers

The worldlines of static observers are the integral curves of the timelike Killing vector field, i.e.

$$u_{(SO)} = \frac{1}{\sqrt{-q_{tt}}} \partial_t . {34}$$

This family of observers exists outside the ergosphere. The SO frame is

$$e_{\mathbf{0}} = u_{(SO)} \ , \ e_{\mathbf{1}} = \sqrt{\frac{\Delta}{\Sigma}} \partial_r \ , \ e_{\mathbf{2}} = \frac{\partial_{\theta}}{\sqrt{\Sigma}} \ ,$$

$$e_{3} = -\frac{1}{\sqrt{\Delta}} \left(\frac{a\mathcal{B}\sin\theta}{\Sigma\sqrt{-g_{tt}}} \partial_{t} - \frac{\sqrt{-g_{tt}}}{\sin\theta} \partial_{\phi} \right) . \tag{35}$$

The dual basis is obtained as $e_a^{\mathbf{A}} = g_{ab}\eta^{\mathbf{A}\mathbf{B}}e_{\mathbf{B}}^b$, where $\eta^{\mathbf{A}\mathbf{B}} = diag(-1, 1, 1, 1)$. The components of the metric in terms of the dual frame basis is $g_{ab} = \eta_{\mathbf{A}\mathbf{B}}e_a^{\mathbf{A}}e_b^{\mathbf{B}}$.

The orbit of a zero angular momentum observer is orthogonal to the t =const. hypersurfaces [92, 93]. The four velocity along this orbit is

$$u_{(ZAMO)} = \sqrt{\frac{A}{\Sigma\Delta}} \left(\partial_t + \frac{aB}{A} \partial_\phi \right) ,$$
 (36)

which corresponds to the 1-form: $-dt/\sqrt{-g^{tt}}$. In contrast to the SOs, this family of observers also exists inside the ergosphere but outside the outer event horizon. The frame of the ZAMOs is given by

$$f_{\mathbf{0}} = u_{(ZAMO)} , f_{\mathbf{1}} = \sqrt{\frac{\Delta}{\Sigma}} \partial_r ,$$

$$f_2 = \frac{\partial_{\theta}}{\sqrt{\Sigma}} , f_3 = \sqrt{\frac{\Sigma}{A}} \frac{\partial_{\phi}}{\sin \theta} ,$$
 (37)

with dual basis: $f_a^{\mathbf{A}} = g_{ab} \eta^{\mathbf{A} \mathbf{B}} f_{\mathbf{B}}^b$.

III. REPRESENTATIONS OF SPIN AND ORBIT EVOLUTIONS

The evolution of the spin vector (7) will be described in comoving frame with the centroid. The spin vector (19) will be considered in both comoving and zero 3-momentum frames. The definitions of comoving and zero 3-momentum observers will be introduced in the next subsection. Then spin evolution equations will be derived using the boosted spatial spherical and Cartesian-like triads. In addition we also define an angular-momentum-like kinematical quantity for characterization of the instantaneous orbital plane.

A. Comoving and zero 3-momentum frames

In the FMP SSC the centroid is measured in the frame with four velocity u^a , i.e. which comoves with it. The centroid is not unique but we can choose one of them, for instance that which moves along a non-helical trajectory. In the TD SSC the center of mass is unique and measured in the zero 3-momentum frame with four velocity p^a/M . The comoving indicative refers to that observer which moves along the chosen centroid worldline, i.e. it has the four velocity u^a . The zero 3-momentum observer has the four velocity p^a/M .

Neither the different centroid four velocities nor p^a/M are given analytically. Below we will refer to these three kinds of four velocities by the notation U, i.e. U = u (in

FMP or in TD SSCs) or $U = p^a/M$ (in TD SSC). The comoving and zero 3-momentum observers' frames will be set up from the frames of the static and the zero angular momentum observers by an instantaneous Lorentz-boost knowing U numerically.

The comoving and zero 3-momentum frames (hereafter unanimously referred as U-frame) obtained from the SO frame are given by

$$E_{\mathbf{0}}(e, U) \equiv U = \Gamma_{(S)} \left(e_{\mathbf{0}} + \mathbf{v}_{(S)} \right) ,$$

$$E_{\alpha}(e, U) = e_{\alpha} + \frac{U \cdot e_{\alpha}}{1 + \Gamma_{(S)}} \left(U + u_{(SO)} \right) . \tag{38}$$

Here $\alpha = \{1, 2, 3\}$, $\mathbf{v}_{(S)}$ is the relative spatial velocity of either the comoving or the zero 3-momentum observer with respect to the SO frame, which is perpendicular to e_0 :

$$\mathbf{v}_{(S)} = \Gamma_{(S)}^{-1} U - u_{(SO)} , \qquad (39)$$

and the Lorentz factor is $\Gamma_{(S)} = -U \cdot u_{(SO)}$. The dot denotes the inner product with respect to the metric g_{ab} , i.e. $W \cdot V \equiv g(W,V) = g_{ab}W^aV^b$ for any vector fields W and V. The inverse transformation is

$$e_{\mathbf{0}} = \Gamma_{(S)} \left(E_{\mathbf{0}} \left(e, U \right) + \mathbf{w}_{(S)} \right) ,$$

$$e_{\alpha} = E_{\alpha}(e, U) + \frac{u_{(SO)} \cdot E_{\alpha}(e, U)}{1 + \Gamma_{(S)}} (U + u_{(SO)}), \quad (40)$$

where

$$\mathbf{w}_{(S)} = w_{(S)}^{\alpha} E_{\alpha} (e, U) = \Gamma_{(S)}^{-1} u_{(SO)} - U , \qquad (41)$$

is the relative spatial velocity of the static observer with respect to the U-frame.

The corresponding Lorentz-boost from the ZAMO frame reads as

$$E_{\mathbf{0}}(f, U) \equiv U = \Gamma_{(Z)} \left(f_{\mathbf{0}} + \mathbf{v}_{(Z)} \right) ,$$

$$E_{\alpha}(f, U) = f_{\alpha} + \frac{U \cdot f_{\alpha}}{1 + \Gamma(Z)} \left(U + u_{(ZAMO)} \right) , \qquad (42)$$

with relative spatial velocity $\mathbf{v}_{(Z)}$ of the *U*-frame with respect to the ZAMO frame:

$$\mathbf{v}_{(Z)} = \Gamma_{(Z)}^{-1} U - u_{(ZAMO)} ,$$
 (43)

and Lorentz factor: $\Gamma_{(Z)} = -U \cdot u^{(ZAMO)}$. The inverse boost transformation is

$$f_{\mathbf{0}} = \Gamma_{(Z)} \left(E_{\mathbf{0}} \left(f, U \right) + \mathbf{w}_{(Z)} \right) ,$$

$$f_{\alpha} = E_{\alpha} \left(f, U \right) + \frac{u_{(ZAMO)} \cdot E_{\alpha} \left(f, U \right)}{1 + \Gamma_{(Z)}} \left(U + u_{(ZAMO)} \right) ,$$

$$(44)$$

where

$$\mathbf{w}_{(Z)} = w_{(Z)}^{\alpha} E_{\alpha}(f, U) = \Gamma_{(Z)}^{-1} u_{(ZAMO)} - U , \qquad (45)$$

is the relative spatial velocity of the ZAMO with respect to either the comoving or the zero 3-momentum frame. Relations between $\mathbf{w}_{(S)}$ and $\mathbf{w}_{(Z)}$ are given in Appendix A

Since $E_{\mathbf{0}}\left(e,U\right)=U=E_{\mathbf{0}}\left(f,U\right)$ the transformation between the frames $E_{\mathbf{A}}\left(e,U\right)$ and $E_{\mathbf{A}}\left(f,U\right)$ is a rotation in the rest space of either the comoving or the zero 3-momentum observer. The rotation axis has the following non-zero components in both the $E_{\mathbf{A}}\left(e,U\right)$ and the $E_{\mathbf{A}}\left(f,U\right)$ frames:

$$n^{1} = -\frac{w_{(Z)}^{2}}{\sqrt{(w_{(Z)}^{1})^{2} + (w_{(Z)}^{2})^{2}}}$$
$$= -\frac{w_{(S)}^{2}}{\sqrt{(w_{(S)}^{1})^{2} + (w_{(S)}^{2})^{2}}}, \qquad (46)$$

and

$$n^{2} = \frac{w_{(Z)}^{1}}{\sqrt{(w_{(Z)}^{1})^{2} + (w_{(Z)}^{2})^{2}}}$$

$$= \frac{w_{(S)}^{1}}{\sqrt{(w_{(S)}^{1})^{2} + (w_{(S)}^{2})^{2}}}.$$
(47)

The second equalities in (46) and (47) come from the relations enlisted in Appendix A. The rotation angle Θ is determined by

$$\sin\Theta = \left[\left(1 - \sqrt{\frac{\Sigma\Delta}{-g_{tt}\mathcal{A}}} \right) \frac{\Gamma_{(Z)}w_{(Z)}^{3}}{1 + \Gamma_{(Z)}} + \frac{a\mathcal{B}\sin\theta}{\sqrt{-g_{tt}\Sigma\mathcal{A}}} \right]$$

$$\times \frac{\Gamma_{(Z)}\sqrt{\left(w_{(Z)}^{1}\right)^{2} + \left(w_{(Z)}^{2}\right)^{2}}}{1 + \Gamma_{(S)}}$$

$$= -\left[\left(1 - \sqrt{\frac{\Sigma\Delta}{-g_{tt}\mathcal{A}}} \right) \frac{\Gamma_{(S)}w_{(S)}^{3}}{1 + \Gamma_{(S)}} - \frac{a\mathcal{B}\sin\theta}{\sqrt{-g_{tt}\Sigma\mathcal{A}}} \right]$$

$$\times \frac{\Gamma_{(S)}\sqrt{\left(w_{(S)}^{1}\right)^{2} + \left(w_{(S)}^{2}\right)^{2}}}{1 + \Gamma_{(Z)}}, \tag{48}$$

and

$$\frac{\cos\Theta - 1}{1 - \sqrt{\frac{\Sigma\Delta}{-g_{tt}\mathcal{A}}}} = \frac{\Gamma_{(Z)}^{2} \left[\left(w_{(Z)}^{1} \right)^{2} + \left(w_{(Z)}^{2} \right)^{2} \right]}{\left(1 + \Gamma_{(S)} \right) \left(1 + \Gamma_{(Z)} \right)}$$

$$= \frac{\Gamma_{(S)}^{2} \left[\left(w_{(S)}^{1} \right)^{2} + \left(w_{(S)}^{2} \right)^{2} \right]}{\left(1 + \Gamma_{(S)} \right) \left(1 + \Gamma_{(Z)} \right)} . \quad (49)$$

The frame $E_{\alpha}\left(e,U\right)$ $\left(E_{\alpha}\left(f,U\right)\right)$ is obtained from $E_{\alpha}\left(f,U\right)\left(E_{\alpha}\left(e,U\right)\right)$ by a rotation with the angle $\Theta\left(-\Theta\right)$

about the axis **n**. The rotation angle Θ exists outside the ergosphere where the terms under the square roots in Eqs. (48) and (49) are positive. The transformation between $E_{\alpha}\left(e,U\right)$ and $E_{\alpha}\left(f,U\right)$ in another form is given in Appendix B. The above transformation is a special case of the Wigner-rotation [94] which was discussed recently in Ref. [95]. However explicit expressions for the rotation between the frames which we denote $E_{\alpha}\left(f,U\right)$ and $E_{\alpha}\left(e,U\right)$ were not presented in [95].

B. MPD spin equations in comoving and zero 3-momentum frames

We investigate three different cases related to the chosen U-frame. When using FMP SSC, $U^a = u^a$, i.e. it means the four velocity of the chosen centroid, and \mathbb{S}^a will denote the spin vector s^a defined in Eq. (7). In the case of TD SSC, $\mathbb{S}^a = S^a$ given by Eq. (19) and we consider two subcases: i) $U^a = p^a/M$, when we work in the zero 3-momentum frame; and ii) $U^a = u^a$ which is the four velocity of the center of mass measured in the zero 3-momentum frame. In all cases the spin vector can be expanded as

$$S = S^{\alpha} E_{\alpha} , \qquad (50)$$

since $\mathbb{S}^{\mathbf{0}} = 0$. Here the spatial frame vector E_{α} in the U-frame denotes either $E_{\alpha}(e, U)$ or $E_{\alpha}(f, U)$ which are obtained by boosting the SO and ZAMO frames, respectively.

The covariant derivative of the spin vector along the integral curve of u is

$$\frac{DS}{d\tau} = \frac{dS^{\alpha}}{d\tau} E_{\alpha} + S^{\alpha} \frac{DE_{\alpha}}{d\tau} . \tag{51}$$

Since the frame vectors are perpendicular to each other, we have

$$E_{\mathbf{A}} \cdot \frac{DE_{\mathbf{B}}}{d\tau} = -E_{\mathbf{B}} \cdot \frac{DE_{\mathbf{A}}}{d\tau} , \qquad (52)$$

for $A \neq B$, and because of the normalization:

$$E_{\mathbf{A}} \cdot \frac{DE_{\mathbf{A}}}{d\tau} = 0 \ . \tag{53}$$

Therefore the covariant derivatives of the spatial frame vectors along the integral curve of u can be expressed as

$$\frac{DE_{\alpha}}{d\tau} = -\left(E_{\mathbf{0}} \cdot \frac{DE_{\alpha}}{d\tau}\right) E_{\mathbf{0}} + \mathbf{\Omega} \times E_{\alpha} , \qquad (54)$$

where the angular velocity Ω is

$$\mathbf{\Omega} = \Omega^{\alpha} E_{\alpha} , \qquad (55)$$

with frame components

$$\Omega^{1} = E_{3} \cdot \frac{DE_{2}}{d\tau} = -E_{2} \cdot \frac{DE_{3}}{d\tau} , \qquad (56)$$

$$\Omega^2 = -E_3 \cdot \frac{DE_1}{d\tau} = E_1 \cdot \frac{DE_3}{d\tau} , \qquad (57)$$

$$\Omega^3 = E_2 \cdot \frac{DE_1}{d\tau} = -E_1 \cdot \frac{DE_2}{d\tau} \ . \tag{58}$$

The cross product in Eq. (54) is defined by

$$\mathbf{\Omega} \times E_{\alpha} = -\varepsilon_{\alpha\beta}{}^{\gamma} \Omega^{\beta} E_{\gamma} , \qquad (59)$$

with Levi-Civita symbol $\varepsilon_{\alpha\beta}^{\gamma}$ in the 3-dimensional Euclidean space whose frame indices are raised and lowered by the 3-dimensional Kronecker δ . With the Levi-Civita symbol Eqs. (56)-(58) read as

$$\Omega^{\alpha} = -\frac{1}{2} \varepsilon^{\alpha\beta\gamma} E_{\beta} \cdot \frac{DE_{\gamma}}{d\tau} \ . \tag{60}$$

Due to Eq. (52), the first term⁴ in (54) can be written as

$$E_{\mathbf{0}} \cdot \frac{DE_{\alpha}}{d\tau} = -E_{\alpha} \cdot \mathbf{a} , \qquad (61)$$

where **a** denotes the acceleration $\mathbf{a} = DE_0/d\tau$. Now the spin equation (51) becomes

$$\frac{DS}{d\tau} = \left(\frac{dS^{\alpha}}{d\tau} + \varepsilon^{\alpha}_{\beta\gamma}\Omega^{\beta}S^{\gamma}\right)E_{\alpha} + (S \cdot \mathbf{a})E_{\mathbf{0}}.$$
 (62)

Finally we take into account the corresponding spin equations (11) or (23) depending on the chosen SSC. When using FMP SSC we find the following evolution equation for the spin vector (7) in comoving frame with the centroid:

$$\frac{ds^{\alpha}}{d\tau} + \varepsilon^{\alpha}_{\beta\gamma} \Omega^{\beta} s^{\gamma} = 0 . {(63)}$$

In the TD SSC and in the zero 3-momentum frame we find a similar form equation for the spin vector (19):

$$\frac{dS^{\alpha}}{d\tau} + \varepsilon^{\alpha}_{\beta\gamma} \Omega^{\beta} S^{\gamma} = 0 . \tag{64}$$

The third case, also related to the TD SSC when considering the evolution of S^{α} in the comoving frame, requires a longer computation. Equations (23) and (62) results in

$$\left(\frac{dS^{\alpha}}{d\tau} + \varepsilon^{\alpha}_{\beta\gamma}\Omega^{\beta}S^{\gamma}\right)E_{\alpha} + \Upsilon = 0 ,$$
(65)

with

$$\Upsilon = \left[(S \cdot \mathbf{a}) u^{\mathbf{A}} - (S \cdot \mathbf{F}) \frac{p^{\mathbf{A}}}{M^2} \right] E_{\mathbf{A}} . \tag{66}$$

⁴ Noting that this term vanishes when the first order spin corrections, i.e. the right hand sides of Eqs. (1) and (2), are neglected (see Ref. [83]).

Using Eqs. (16) and (22) a straightforward computation shows that $u \cdot \Upsilon = 0$. Therefore Υ can be expanded as

$$\Upsilon = \Upsilon^{\alpha} E_{\alpha} . \tag{67}$$

On the other hand Υ is also perpendicular to S, thus we can introduce a vector ω as

$$\omega \times S = \Upsilon$$
 (68)

The vector ω is determined ambiguously since its frame component parallel with S vanishes in the cross product. As a natural choice, we choose ω to be perpendicular to S. Using the definition (68), Eq. (65) reads as

$$\frac{dS^{\alpha}}{d\tau} + \varepsilon^{\alpha}_{\beta\gamma} \left(\Omega^{\beta} + \omega^{\beta} \right) S^{\gamma} = 0 . \tag{69}$$

The above equations (63), (64) and (69) can be considered in either the $E_{\alpha}\left(e,U\right)$ or the $E_{\alpha}\left(f,U\right)$ frame. Introducing the notations

$$k = \{e, f\} ,$$

$$\Gamma = \{\Gamma_{(S)}, \Gamma_{(Z)}\} ,$$
(70)

the components of $\Omega^{\alpha}\left(k,U\right)$ can be expressed as

$$E_{\beta}(k,U) \cdot \frac{DE_{\alpha}(k,U)}{d\tau}$$

$$= k_{\beta} \cdot \frac{Dk_{\alpha}}{d\tau} + \frac{1}{1+\Gamma} [(U \cdot k_{\alpha}) k_{\beta}$$

$$- (U \cdot k_{\beta}) k_{\alpha}] \cdot \frac{Dk_{\mathbf{0}}}{d\tau} + \frac{1}{1+\Gamma}$$

$$\times [(U \cdot k_{\alpha}) k_{\beta} - (U \cdot k_{\beta}) k_{\alpha}] \cdot \frac{DU}{d\tau} , \qquad (71)$$

where $\alpha \neq \beta$. This can be computed once *U* is determined.

We note that when the right hand sides of Eqs. (1) and (2) are neglected, the centroid moves along a geodesic thus ω and the last term in (71) vanish. The four-velocity U is determined from the geodesic equation and for k=e we obtain the same system which was investigated in Ref. [83].

C. Cartesian-like triads and the characterizations of orbit and spin evolutions

The evolution of the spin vector can be illustrated suitably by comparison its direction with Cartesian axes which are fixed with respect to the distant stars. The static observers are those fiducial observers whose frame does not move with respect to the black hole's asymptotic frame [96]. A static observer sees the same "nonrotating" sky during the evolution. In this sense the static observers are preferred fiducial observers in the investigation of spin dynamics. Following Ref. [83], we introduce a spatial Cartesian-like triad $e_{\mathbf{x}}$, $e_{\mathbf{y}}$ and $e_{\mathbf{z}}$ in the local rest space of the static observer as

$$(e_1, e_2, e_3) = (e_x, e_y, e_z) R_{(e)},$$
 (72)

where $R_{(e)}$ is the same rotation matrix which relates the Cartesian and spherical coordinates in the 3-dimensional Euclidean space, see Eq. (85) of [83]. The spinning body's orbit will be represented in the coordinate space:

$$x = r \cos \phi \sin \theta ,$$

$$y = r \sin \phi \sin \theta ,$$

$$z = r \cos \theta .$$
 (73)

We characterize the instantaneous plane of the motion in the (x, y, z)-space by the unit vector:

$$1 = \frac{\mathbf{R} \times \mathbf{V}}{|\mathbf{R} \times \mathbf{V}|} \,, \tag{74}$$

where \times is the cross product in Euclidean 3-space, \mathbf{R} is the position vector with components:

$$R^{\mathbf{x}} = x , R^{\mathbf{y}} = y , R^{\mathbf{z}} = z ,$$
 (75)

and ${\bf V}$ is a spatial velocity vector with⁵

$$V^{\mathbf{x}} = \frac{dx}{d\tau} , V^{\mathbf{y}} = \frac{dy}{d\tau} , V^{\mathbf{z}} = \frac{dz}{d\tau} .$$
 (76)

The absolute value in the denominator denotes the "Euclidean length" of the numerator. Since the considered spacetimes are asymptotically flat, the quantity l^{i} coincides with the direction of the orbital angular momentum⁶ at spatial infinity.

Boosting the vectors e_{α} to the *U*-frame we get $E_{\alpha}(e,U)$ through Eq. (38). Applying the same boost transformation for $e_{\mathbf{i}}$ we have $E_{\mathbf{i}}(e,U)$. Since the rotation $R_{(e)}$ and the boost can be interchanged, we find

$$(E_1, E_2, E_3)(e, U) = (E_x, E_y, E_z)(e, U) R_{(e)}$$
 (77)

The family of static observers only determines a frame outside the ergosphere. Therefore we introduce another Cartesian-like basis related to the ZAMOs for representation of the spin evolution inside the ergosphere. When both SO and ZAMO frames exist, a rotation about the axis $\bf n$ defined by Eqs. (46) and (47) [see also Appendix B for the explicit expressions] relates $E_{\alpha}(f, U)$ to $E_{\alpha}(e, U)$ which can be written as

$$(E_1, E_2, E_3) (f, U) \mathcal{R} = (E_1, E_2, E_3) (e, U)$$
 (78)

$$L^{ab} = -\sigma^{[a}(x, x_0) p^{b]}(\tau)$$
.

Here σ^a is a generalized position vector which can be computed from the Synge's world function [97]. However there are only few metrics for which the exact world function is known [98–104].

Noting that we could use any timelike parameter in the definition (76) due to the normalisation in Eq. (74).

⁶ We mention that the natural definition of orbital angular momentum around x_0 would be

⁷ Noting that the frame associated to the ZAMO moves with respect to the distant stars.

Here \mathcal{R} denotes the corresponding rotation matrix. Similarly to the case of SO, we introduce a spatial Cartesian-like triad $f_{\mathbf{x}}$, $f_{\mathbf{y}}$ and $f_{\mathbf{z}}$ in the rest space of ZAMO as

$$(f_1, f_2, f_3) = (f_x, f_y, f_z) R_{(f)},$$
 (79)

where $R_{(f)}$ is the same rotation matrix which relates the Cartesian and spherical coordinates in the 3-dimensional Euclidean space. After boosting the ZAMO frame we find

$$(E_1, E_2, E_3)(f, U) = (E_x, E_y, E_z)(f, U)R_{(f)}$$
. (80)

Here $E_{\alpha}(f, U)$ and $E_{\mathbf{i}}(f, U)$ are the boosted vectors f_{α} and $f_{\mathbf{i}}$, respectively. The relation between the Cartesian-like frame vectors $E_{\mathbf{i}}(e, U)$ and $E_{\mathbf{i}}(f, U)$ is

$$(E_{\mathbf{x}}, E_{\mathbf{y}}, E_{\mathbf{z}}) (f, U) R_{(f)} \mathcal{R} = (E_{\mathbf{x}}, E_{\mathbf{y}}, E_{\mathbf{z}}) (e, U) R_{(e)}.$$
(81)

The Cartesian-like triad components of the spin vector are obtained as

$$S^{\mathbf{i}} = R^{\mathbf{i}}{}_{\alpha}S^{\alpha} , \qquad (82)$$

where R refers to either $R_{(e)}$ or $R_{(f)}$ depending on the chosen basis pairs $E_{\alpha}\left(e,U\right)$ and $E_{\mathbf{i}}\left(e,U\right)$ or $E_{\alpha}\left(f,U\right)$ and $E_{\mathbf{i}}\left(f,U\right)$, respectively. The evolution equation for $\mathbb{S}^{\mathbf{i}}$ is

$$\frac{dS^{\mathbf{i}}}{d\tau} = -R^{\mathbf{i}}{}_{\alpha} \varepsilon^{\alpha}{}_{\beta\gamma} \Omega^{\beta}_{(prec)} S^{\gamma} . \tag{83}$$

Here the precession angular velocity is⁸

$$\Omega_{(nrec)}^{\beta} = \Omega_{(n)}^{\beta} + \epsilon \omega^{\beta} , \qquad (84)$$

with

$$\Omega_{(p)}^{\beta} = -\Omega_{(orb)}^{\beta} + \Omega^{\beta} , \qquad (85)$$

where $\Omega^{\beta}_{(orb)}$ defined [see also Ref. [83]] as

$$(R^{-1})^{\alpha}_{\mathbf{j}} \frac{dR^{\mathbf{j}}_{\beta}}{d\tau} = \varepsilon^{\alpha}_{\gamma\beta} \Omega^{\gamma}_{(orb)} , \qquad (86)$$

and the values of ϵ are listed in Table I. The quantity

Table I: The meaning of S and ϵ in Eqs. (83) and (84), respectively, in different SSCs and the related U-frames.

FMP SSC	TD SSC	
$U^a = u^a$	$U^a = p^a/M$	$U^a = u^a$
$\mathbb{S} = s \; , \; \epsilon = 0$	$\mathbb{S} = S \; , \; \epsilon = 0$	$\mathbb{S} = S, \ \epsilon = 1$

 $\Omega_{(prec)}^{\beta}$ describes the spin precession in the Cartesian-like frame. The Cartesian-like triad components of $\Omega_{(prec)}^{\beta}$ are obtained from Eq. (82) with notation change $\mathbb{S} \to \Omega_{(prec)}$. In addition we note that $\Omega_{(p)}$ can also be expressed in terms of the inner product of the Cartesian-like triad vectors $E_{\mathbf{i}}$ and their derivatives along the considered worldline as

$$\Omega_{(p)}^{\mathbf{i}} \equiv R^{\mathbf{i}}{}_{\beta} \Omega_{(p)}^{\beta} = -\frac{1}{2} \varepsilon^{\mathbf{i}\mathbf{j}\mathbf{k}} E_{\mathbf{j}} \cdot \frac{DE_{\mathbf{k}}}{d\tau} .$$
(87)

This expression is analogous with Eq. (60).

1. Relations between the angular velocities in the boosted SO and ZAMO frames

The relation between $E_{\alpha'}(f,U)$ and $E_{\alpha}(e,U)$ is $E_{\beta}(e,U) = \mathcal{R}_{\beta}^{\alpha'} E_{\alpha'}(f,U)$ (see also (78)), where the rotation matrix \mathcal{R} is obtained from (B2). In this subsubsection the primed and unprimed indices refer to the triads $E_{\alpha'}(f,U)$ and $E_{\alpha}(e,U)$, respectively. Two kinds of Cartesian-like frame vectors were introduced as $E_{\alpha}(e,U) = R_{(e)\alpha}^{\mathbf{i}} E_{\mathbf{i}}(e,U)$ and $E_{\alpha'}(f,U) = R_{(f)\alpha'}^{\mathbf{i}'} E_{\mathbf{i}'}(f,U)$ (see Eqs. (77) and (80)). The relation between the Cartesian-like bases is

$$\left(R_{(e)}^{-1}\right)_{\mathbf{k}}^{\beta} \mathcal{R}_{\beta}^{\alpha'} R_{(f)\alpha'}^{\mathbf{i}'} E_{\mathbf{i}'}\left(f, U\right) = E_{\mathbf{k}}\left(e, U\right) . \tag{88}$$

When using the frame vectors $E_{\alpha}\left(e,U\right)$ and $E_{\mathbf{i}}\left(e,U\right)$, Eqs. (60) and (87) define angular velocities $\Omega^{\alpha}\left(e,U\right)$ and $\Omega^{\mathbf{i}}_{(p)}\left(e,U\right)$, respectively, as

$$\Omega^{\alpha}(e, U) = -\frac{1}{2} \varepsilon^{\alpha\beta\gamma} E_{\beta}(e, U) \cdot \frac{DE_{\gamma}(e, U)}{d\tau} , \qquad (89)$$

$$\Omega_{(p)}^{\mathbf{i}}(e, U) = -\frac{1}{2} \varepsilon^{\mathbf{i}\mathbf{j}\mathbf{k}} E_{\mathbf{j}}(e, U) \cdot \frac{DE_{\mathbf{k}}(e, U)}{d\tau} . \tag{90}$$

Similarly, with the frame vectors $E_{\alpha'}(f, U)$ and $E_{\mathbf{i}'}(f, U)$ Eqs. (60) and (87) give $\Omega^{\alpha'}(f, U)$ and $\Omega^{\mathbf{i}'}_{(p)}(f, U)$, respectively:

$$\Omega^{\alpha'}(f,U) = -\frac{1}{2} \varepsilon^{\alpha'\beta'\gamma'} E_{\beta'}(f,U) \cdot \frac{DE_{\gamma'}(f,U)}{d\tau} , \quad (91)$$

$$\Omega_{(p)}^{\mathbf{i}'}(f,U) = -\frac{1}{2} \varepsilon^{\mathbf{i}'\mathbf{j}'\mathbf{k}'} E_{\mathbf{j}'}(f,U) \cdot \frac{DE_{\mathbf{k}'}(f,U)}{d\tau} . \tag{92}$$

In addition the definition (86) results in

$$\left(R_{(e)}^{-1}\right)^{\varphi}_{\mathbf{m}} \frac{DR_{(e)\phi}^{\mathbf{m}}}{d\tau} = \varepsilon^{\varphi}_{\psi\phi} \Omega_{(orb)}^{\psi} \left(e, U\right) , \quad (93)$$

$$\left(R_{(f)}^{-1}\right)_{\mathbf{m}'}^{\varphi'} \frac{DR_{(f)\delta'}^{\mathbf{m}'}}{d\tau} = \varepsilon_{\psi'\delta'}^{\varphi'} \Omega_{(orb)}^{\psi'}(f, U) .$$
(94)

⁸ Noting that there is a sign difference in the definition of $\Omega^{\beta}_{(prec)}$ with respect to Ref. [83].

By introducing the angular velocity $\Omega_{(\mathcal{R})}^{\gamma}$ as

$$\left(\mathcal{R}^{-1}\right)^{\alpha}_{\nu'}\frac{d\mathcal{R}^{\nu'}_{\beta}}{d\tau} = \varepsilon^{\alpha}_{\gamma\beta}\Omega^{\gamma}_{(\mathcal{R})}, \qquad (95)$$

we find the following relation between $\Omega^{\alpha}\left(e,U\right)$ and $\Omega^{\beta'}\left(f,U\right)$:

$$\mathcal{R}_{\alpha}^{\beta'}\Omega^{\alpha}\left(e,U\right) = \Omega^{\beta'}\left(f,U\right) + \mathcal{R}_{\alpha}^{\beta'}\Omega_{(\mathcal{R})}^{\alpha}.$$
 (96)

In addition $\Omega_{(p)}^{\mathbf{i}}\left(e,U\right)$ relates to $\Omega_{(p)}^{\mathbf{k}'}\left(f,U\right)$ as

$$\begin{split} T^{\mathbf{k}'}_{\mathbf{i}} \Omega^{\mathbf{i}}_{(p)} \left(e, U \right) + S^{\mathbf{k}'}_{\alpha} \Omega^{\alpha}_{(orb)} \left(e, U \right) \\ &= \Omega^{\mathbf{k}'}_{(p)} \left(f, U \right) + R^{\mathbf{k}'}_{(f) \, \beta'} \Omega^{\beta'}_{(orb)} \left(f, U \right) + S^{\mathbf{k}'}_{\alpha} \Omega^{\alpha}_{(\mathcal{R})} , (97) \end{split}$$

with

$$T_{\mathbf{i}}^{\mathbf{k}'} \equiv \left(R_{(e)}^{-1}\right)_{\mathbf{i}}^{\beta} \mathcal{R}_{\beta}^{\alpha'} R_{(f)\alpha'}^{\mathbf{k}'} , \qquad (98)$$

$$S^{\mathbf{k'}}_{\alpha} \equiv R^{\mathbf{k'}}_{(f)\beta'} \mathcal{R}^{\beta'}_{\alpha} .$$
 (99)

Noting that ω^{α} in Eq. (68) transforms as a vector for real rotation $\mathcal{R}^{\beta'}_{\alpha}$, the transformation rules for $\Omega^{\beta}_{(prec)}$ and $\Omega^{\mathbf{i}}_{(prec)}$ follow from the definitions (84) and (97).

IV. NUMERICAL INVESTIGATIONS

First we use the FMP SSC and the spin definition (7). In this SSC, there are infinite helical orbits which can be obtained. Since the tangent vector of the centroid orbit occurs in the spin precessional equation through $E_{\mathbf{A}}$ and their derivatives, the spin axis can describe very complicated motion in such observer's frame which follows a helical trajectory. Since we want to characterize the self rotation of the body in the easiest way possible the helical trajectories should be avoided. However there is no generic rule for determination of the non-helical trajectory. According to Authors' knowledge the best ansatz is suggested in Ref. [86] as taking

$$p^a = mu^a + S^{ab} \frac{F_b}{m} . ag{100}$$

In this case $a^a \propto F^a/m$ at leading order in spin which is plausible for a non-helical trajectory since $a^a \propto \mathcal{O}\left(S^{-1}\right)$ for the helical ones. However the ansatz (100) cannot be imposed as a constraint for the dynamics with significant spin magnitude in the consideration. We require the ansatz (100) for setting initial conditions in the numerical investigations. This is not forbidden because (100) is consistent with (13) which can be seen by substituting (100) in (13) and using the FMP SSC.

The initial data for the spin vector will be characterized by its magnitude and two angles in the boosted SO Cartesian-like frame as

$$S = S^{\mathbf{i}} E_{\mathbf{i}} (e, u) , \qquad (101)$$

with

$$\mathbb{S}^{\mathbf{i}} = |\mathbb{S}| \left(\cos \phi^{(S)} \sin \theta^{(S)}, \sin \phi^{(S)} \sin \theta^{(S)}, \cos \theta^{(S)} \right). \tag{102}$$

When comparing the evolutions in the TD and the FMP SSCs we proceed as follow. First noting that we use dimensionless quantities during the numerical investigation. Thus the parameters μ , a, m and M only appear through the ratios a/μ and m/M. We choose the initial data set in the TD SSC as $p_{(TD)}^a/M$ and $S^a/\mu M$ (by Eq. (102)) then the initial spin tensor is derived from Eq. (20) while m(0)/M(0) and the four velocity $u_{(TD)}^a$ of the centroid from (16), respectively. The corresponding initial data set in the FMP SSC are chosen by identifying the initial centroid four velocity and spin vector as $u^a_{(FMP)} = u^a_{(TD)}$ and $s^a/m = S^a/M$. Then the initial spin tensor and $p_{(FMP)}^a/m$ are computed from Eqs. (8) and (100), respectively. In addition in all cases who choose such initial conditions that the body moves in the equatorial plane for negligible spin magnitude.

A. Spinning bodies moving in the Kerr spacetime

In this subsection we set $\mu_{em} = 0$ and $a/\mu < 1$, i.e. the background is a Kerr black hole's spacetime. Figure 1 shows spherical-like orbits. The initial values are listed in the caption. The orbits, the black curves in the upper row, are shown in the coordinate space $(x/\mu,y/\mu,z/\mu)$ defined in Eq. (73). The initial and the final positions of the body are marked by green and red dots, respectively. The initial position is in the equatorial plane $\theta(0) = \pi/2$ at $r(0) = 8\mu$ and $\phi(0) = 0$. The blue surface at the centre depicts the outer bound of the Kerr black hole's ergosphere. In the columns from left to right the spin magnitude $|s|/\mu m$ changes as 0.01, 0.1 and 0.9, respectively, while the other initial values are fixed. For small spin the orbit is spherical $(\dot{r}=0)$ and reproduces Fig. 3 of [83]. For higher spins (second and third columns) the orbit becomes less and less spherical, but $\dot{r} \ll 1$, thus it is spherical-like. On the purplish spheres in the second row, the evolutions of the kinematical quantity defined in Eq. (74) are shown under the corresponding orbits. Their initial and final directions are marked by purple and black arrows, respectively. The evolutions of this vector clearly show that the increasing spin magnitude affects the orbit. On the greenish spheres in the third row, the evolutions of the spin direction are represented in the boosted SO frame $E_{\mathbf{i}}(e, u)$. The initial and final spin directions are marked by green and blue arrows, respectively. In Boyer-Lindquist coordinates the initial spin four vector s^a has only non-vanishing component s^r . The fourth and fifth rows image the evolutions of spin precessional angular velocity $\Omega_{(prec)}^{\alpha}(e,u)$ on shorter and longer timescales, respectively. For $|s|/\mu m = 0.01$, the frame components of this angular velocity oscillates (see also Fig. 3 of Ref. [83] and remembering for that the definition of $\Omega_{(nrec)}^{\beta}$ carries an extra sign). For $|s|/\mu m=0.1$ and 0.9, an amplitude modulation occurs because of $\dot{r}\neq 0$. We mention that the evolution of $\Omega^{\alpha}_{(prec)}(f,u)$ differs less than 1% from that of $\Omega^{\alpha}_{(prec)}(e,u)$. This is because the boosted SO and ZAMO frames are almost the same, i.e. the rotation angle Θ between them is small as shown in the last row. The centroid orbit and the spin vector evolutions were also investigated in the TD SSC finding that they are barely distinguishable from those obtained in the FMP SSC. In addition all precessional angular velocities $\Omega^{\alpha}_{(prec)}(e,p/M)$, $\Omega^{\alpha}_{(prec)}(e,u)$, $\Omega^{\alpha}_{(prec)}(f,p/M)$ and $\Omega^{\alpha}_{(prec)}(f,u)$ in the frames $E_{\alpha}(e,p/M)$, $E_{\alpha}(e,u)$, $E_{\alpha}(f,p/M)$ and $E_{\alpha}(f,u)$, respectively, describe the same evolutions within 1%.

In the followings, we will consider zoom-whirl orbits passing over the ergosphere. We use the TD SSC because we experienced that the MPD equations with this SSC have better numerical stability near the central On Fig. 2 the first row shows the orbits in the (x,y,z)-space for increasing spin magnitude $|S|/\mu M = 0.01$ (left panel) and 0.1 (right panel). The other initial values listed in the caption are the same for all cases. The blue and red surfaces at the centre depict the outer and interior bounds of the ergosphere, respectively (i.e. the outer stationary limit surface and the outer event horizon). The initial and final positions of the body are marked by green and red dots, respectively. The initial position is in the equatorial plane $\theta(0) = \pi/2$ at $r(0) = 14.05\mu$ and $\phi(0) = 0$, and both the initial four momentum and centroid four velocity have vanishing θ -component. With this initial location and four velocity a non-spinning particle moves in the equatorial plane. However due to the spin and its direction which is non parallel with the rotation axis of the central black hole, the body's centroid leaves the equatorial plane. The second row represents the orbits in coordinates $\rho/\mu = r \sin \theta/\mu$ and $z/\mu = r \cos \theta/\mu$. The bounds of the ergosphere are drawn by blue and red curves. The body is inside there ergosphere when it whirls around the central Kerr black hole. This happens during all whirling period. In the third row, we show the orientation of the orbital plane, the characterizing kinematical quantity is a quasi-constant for small spin (the motion of the body is almost constrained to the equatorial plane), while its endpoint describes a leaf structure evolution on the unit sphere for higher spin. The unit spin vector evolutions on a shorter timescale and on the total considered timescale in the boosted SO Cartesian-like comoving frame $(E_{\mathbf{i}}(e,u))$ are shown in the fourth and the fifth rows, respectively. The initial and final directions are marked by green and blue arrows, respectively. The rotation of the projection of spin vector in the plane $(E_{\mathbf{x}}(e,u), E_{\mathbf{y}}(e,u))$ is counterclockwise in all cases. In the boosted SO frame the evolution is not continuous due to the motion through the ergosphere. The black dots denote the spin directions when the body first enters and leaves the ergosphere. The magnitude of the jump (which can be seen better in the fourth row) shows that the

spin direction changed significantly inside the ergosphere. The sixth row shows the unit spin vector evolution on the total timescale in the boosted ZAMO Cartesian-like comoving frame $(E_{\mathbf{i}}(f, u))$. This frame can be used for the spin representation inside the ergosphere thus the evolution is continuous. The first row in Fig. 3 shows the rotation angle Θ between the boosted SO and ZAMO frames. Here and in the following pictures the purplish shadow indicates the time interval where the body moves inside the ergosphere during the first whirling period. The next three rows in Fig. 3 depict the evolutions of $\Omega_{(prec)}^{\alpha}(e,u)$ and $\Omega_{(prec)}^{\alpha}(f,u)$. Each row shows one component of these angular velocities. The red and blue curves represent the precessional angular velocities in the boosted ZAMO and SO frames, respectively. The blue curves diverge at the ergosphere where the description in the boosted SO frame fails. The magnitude of the precessional angular velocities rapidly increases near and inside the ergosphere and becomes higher for higher spin magnitude. Finally, we note that the precessional velocities $\Omega_{(prec)}^{\alpha}\left(e,p/M\right)\left(\Omega_{(prec)}^{\alpha}\left(f,p/M\right)\right)$ and $\Omega_{(prec)}^{\alpha}\left(e,u\right)$ $\left(\Omega_{(prec)}^{\alpha}\left(f,u\right)\right)$ describe the same evolutions within 1%.

On Fig. 4 the initial direction of the spin vector is opposite with respect to the case presented in the second column of Figs. 2 and 3, while all other initial conditions are the same (e.g. $|S|/\mu M=0.1$). All subfigures on Fig. 4 can be obtained by simple transformations from the corresponding pictures shown on the last columns of Figs. 2 and 3. The centroid trajectory is the reflection of the orbit presented on Fig. 2 through the equatorial plane. The instantaneous directions of l^i (third panel) and the spin vector in the boosted SO (ZAMO) frame are obtained from the corresponding picture of Fig. 2 by a rotation with an angle π about the axis z and $E_z(e,u)$ ($E_z(f,u)$), respectively. The angle Θ describes the same evolution. The components $\Omega^2_{(prec)}(e,u)$ and $\Omega^2_{(prec)}(f,u)$ remain unchanged while $\Omega^1_{(prec)}(e,u)$, $\Omega^1_{(prec)}(f,u)$, $\Omega^3_{(prec)}(e,u)$ and $\Omega^3_{(prec)}(f,u)$ get extra signs.

On Fig. 5 the initial spin direction is rotated by $\pi/2$ (left column) and $-\pi/2$ (right column) in the plane $(E_{\mathbf{x}}(e,u), E_{\mathbf{y}}(e,u))$ with respect to the case presented on Fig. 2. These two cases have opposite initial spin directions leading to similar differences in the orbit and spin evolutions which were found between the previous cases presented in the last columns of Figs. 2, 3 and 4. The zoom-whirl orbit on the right hand side is the reflection of the trajectory on the left hand side through the equatorial plane. The third row shows the evolution of l^{i} . The fourth and fifth rows show the unit spin vector evolution on a shorter timescale and on the total timescale in the boosted SO Cartesian-like comoving frame. Finally, the sixth row shows the unit spin vector evolution on the total timescale in the boosted ZAMO Cartesian-like comoving frame. From the third to sixth rows the evolutions presented on the left and the right hand sides are related to each other by a rotation with an angle π about the axis connecting the south and north poles. On Fig. 6 the rows image Θ and $\Omega^{\alpha}_{(prec)}$ (e,u) and $\Omega^{\alpha}_{(prec)}$ (f,u). The evolutions of Θ and $\Omega^{\mathbf{2}}_{(prec)}$ are the same on the left and right hand sides, while $\Omega^{\mathbf{1}}_{(prec)}$ and $\Omega^{\mathbf{3}}_{(prec)}$ have a sign difference. In addition noting that there is no simple transformation between the evolutions presented on Figs. 5 (6) and 2 (3).

We consider the evolutions of spinning bodies which follow unbound orbits crossing through the ergosphere. The spin magnitude is chosen as $|S|/\mu M = 0.1$. The initial spin directions on the left (right) hand side of Fig. 7 are the same as on Fig. 2 (on the left hand side of Fig. 5). The first row depicts the unbound orbits in the (x,y,z)-space. The initial data set is chosen at $r(\tau = 0) = 2000\mu$ where the body is in the equatorial plane $(\theta(\tau = 0) = \pi/2 \text{ and } \phi(\tau = 0) = 0)$ and the centroid four velocity has vanishing θ -component. We numerically checked that $r \to \infty$ as $\tau \to \pm \infty$. Second and third rows represent the orbits near the black hole in the (x,y,z) and the (ρ,z) spaces, respectively. The interval for τ is determined by -5μ before and $+5\mu$ after the body crossed the outer stationary limit surface. As the body penetrates the ergosphere it makes two turns around the black hole, then it leaves the ergosphere going to the spatial infinity. These evolutions describe such scattering processes where the center is extremely approached. The fourth, fifth and sixth rows image the evolutions of the instantaneous orbital plane orientation and spin vector represented in the boosted SO and ZAMO frames, respectively. The jump in the evolution of the spin vector in the boosted SO frame (marked by black dots) shows that the variation of spin direction takes place largely inside the ergosphere. In both columns the initial 1(0) is parallel with the coordinate axis z. The polar and azimuthal angles of 1 at $\tau^* = 4433\mu$ when the body moved away from the central black hole are denoted by $\theta^{(l)}(\tau^*)$ and $\phi^{(l)}(\tau^*)$. For $\tau > \tau^*$ these angles undergoes only unsignificant changes, thus they characterize the scattering process well. In the presented two cases only the values of $\phi^{(l)}(\tau^*)$ is different, see the caption. On Fig. 8, the evolutions of Θ and $\Omega_{(prec)}^{\alpha}\left(e,u\right)$ and $\Omega_{(prec)}^{\alpha}\left(f,u\right)$ are presented for that time interval which is determined by -25μ before and $+25\mu$ after the body crossed the outer stationary limit surface. As previously, Θ is small when the body is relatively far from the black hole. In addition the spin precessional velocities are highly increased near the ergosphere.

B. Spinning bodies moving in rotating regular black hole spacetimes

In this subsection we set $\mu=0, \gamma=3$ and $a=0.99\mu_{em}$. The background is either a regular, rotating Bardeen-like $(\nu=2)$ or Hayward-like $(\nu=3)$ black hole spacetime. For $\nu=2$ and $\nu=3$ the spacetime contains a black hole

for $q \leq 0.081$ and $q \leq 0.216$, respectively. We consider three cases: $(\nu = 2, q = 0.081)$, $(\nu = 3, q = 0.081)$ and $(\nu = 3, q = 0.216)$. For these parameters the regular black holes have two stationary limit surfaces and event horizons. In addition the spin magnitude for the moving body is chosen as $|S|/\mu M = 0.1$.

On Fig. 9 zoom-whirl orbits in regular rotating black hole spacetimes are presented. The columns from left to right correspond to $(\nu = 2, q = 0.081), (\nu = 3, q = 0.081)$ and $(\nu = 3, q = 0.216)$. With the notation change $\mu \to \mu_{em}$, the initial values are chosen the same as in the second column of Fig. 2. Each row represents the same quantity which was shown on Fig. 2. The first two columns show that both the orbit and the spin evolutions are significantly different in the cases of the Bradeen-like and Hayward-like black holes for the same μ_{em} and qvalues. In addition the second and the third columns show in the case of Hayward-like background that these evolutions are also sensitive for the value of q. On Fig. 10 the evolutions of the angle Θ and the frame components of the spin precessional angular velocities are represented during the time interval containing the first three whirling period. The magnitudes of the components of the precessional angular velocity take somewhat different values in the different columns during the whirling periods.

On Figs. 11 and 12, evolutions along unbound orbits in regular rotating black hole spacetimes are shown. In the columns from left to right the values for the parameter pair (ν,q) are chosen the same as on Fig. 9. With the notation change $\mu \to \mu_{em}$, the initial values are chosen the same as in the second column of Fig. 7. On Figs. 11 and 12, each row represents the same quantity which was given on Figs. 7 and 8, respectively. The evolutions are different on Bardeen-like and Hayward-like backgrounds for the same μ_{em} and q values. The scattering process also depends on the value of q as we can see from the second and third columns in the case of Hayward-like background. Interestingly the evolutions show more similarities to each other in the cases ($\nu = 2, q = 0.081$) and $(\nu = 3,q = 0.216)$ than in the cases $(\nu = 3,q = 0.081)$ and $(\nu = 3, q = 0.081)$. The angles $\theta^{(S)}(\tau^*)$ and $\phi^{(S)}(\tau^*)$ characterizing the spin direction in the boosted SO frame at τ^* undergoes only unsignificant variation for $\tau > \tau^*$. Thus these angles also characterize the result of the scattering process well. In considered three cases significant variation occurs only in the value of $\phi^{(S)}(\tau^*)$, see the caption of Fig. 11. In addition the values of $\theta^{(S)}(\tau^*)$ and $\phi^{(S)}(\tau^*)$ for $(\nu = 3, q = 0.081)$ are almost the same as in the case presented in the second column of Fig. 7 (see the captions of Figs. 7 and 11). Similar statements are also valid for $\theta^{(l)}(\tau^*)$ and $\phi^{(l)}(\tau^*)$ characterizing the final value of the orbital plane evolution in the coordinate space (x,y,z).

V. CONCLUDING REMARKS

We derived spin evolution equations in different U-frames based on the MPD equations with FMP and TD SSCs. When using FMP SSC the centroid is measured in that frame which comoves with it. The centroid is not unique, we chose that which moved along a non-helical trajectory in order to describe the motion of the body's spin in the easiest way possible. The spin is defined in (7) and its evolution is described in the comoving frame $(U^a = u^a)$ by Eq. (63). When using TD SSC the centroid is unique and it is measured in the zero 3-momentum frame $U^a = p^a/M$. The spin vector is defined in (19) and its evolution is described in the zero 3-momentum frame $U^a = p^a/M$ by Eq. (64) and in the comoving frame $U^a = u^a$ by Eq. (69).

For a chosen U-frame two subframes were set up differing from each other by an instantaneous space-like rotation. These subframes were obtained by boost transformations from either the SO or the ZAMO frames. Since the SO are not moving with respect to the distant stars, Cartesian-like basis vectors in its rest space give good reference directions to which the spin vector evolution can be compared. However if the body passes over the ergosphere the boosted SO frame cannot be used for description of the dynamics during the whole evolution. Instead the boosted ZAMO frame remains applicable. Noting that the ZAMO's frame has no such good properties as the SO's, since the ZAMO rotates with respect to the distant stars. We described the spin dynamics in two Cartesian-like U-frames (see Eq. (83)) related to the SO and the ZAMO.

The spin equations were applied for numerical considerations when the spinning body moved along sphericallike, zoom-whirl and unbound orbits. When the spacetime curvature and the spin contributions on the right hand sides of the MPD equations can be neglected we recovered the corresponding results of Ref. [83] for a spherical orbit. However increasing the spin magnitude and/or approaching the centre, the orbit becomes non-geodesic leaving a trace in the spin precession.⁹ The existence of zoom-whirl orbits are confirmed by using the MPD dynamics. The presented zoom-whirl and unbound orbits of spinning body passed over the ergosphere where the PN approximation cannot be applied. In all cases the numerical investigations showed that the spin precessional angular velocity highly increased near and inside the ergosphere. Thus the direction of the spin vector is significantly variated during the evolutionary phase inside the ergosphere.

VI. ACKNOWLEDGEMENTS

The work of Z. K. was supported by the János Bolyai Research Scholarship of the Hungarian Academy of Sciences, by the UNKP-18-4 New National Excellence Program of the Ministry of Human Capacities and by the Hungarian National Research Development and Innovation Office (NKFI) in the form of the grant 123996. The work of B. M. was supported by the Hungarian National Research Development and Innovation Office (NKFI) in the form of the grant 116892 and by the János Bolyai Research Scholarship of the Hungarian Academy of Sciences.

Appendix A: Relations between $w_{(S)}^{\alpha}$ and $w_{(Z)}^{\alpha}$

Here we enlist some relations between the relative spatial velocities of the SO and ZAMO with respect to either the comoving or the zero 3-momentum frame (depending on the meaning of U which occurs in the Lorentz factors):

$$\Gamma_{(S)}w_{(S)}^{\mathbf{1}} = \Gamma_{(Z)}w_{(Z)}^{\mathbf{1}}, \qquad (A1)$$

$$\Gamma_{(S)}w_{(S)}^2 = \Gamma_{(Z)}w_{(Z)}^2$$
, (A2)

$$\Gamma_{(Z)} w_{(Z)}^{3} = \Gamma_{(S)} \left[\frac{a \mathcal{B} \sin \theta}{\sqrt{-g_{tt} \Sigma \mathcal{A}}} + \sqrt{\frac{\Sigma \Delta}{-g_{tt} \mathcal{A}}} w_{(S)}^{3} \right] , \quad (A3)$$

$$-\Gamma_{(S)}w_{(S)}^{3} = \Gamma_{(Z)} \left(\frac{a\mathcal{B}\sin\theta}{\sqrt{-g_{tt}\Sigma\mathcal{A}}} - \sqrt{\frac{\Sigma\Delta}{-g_{tt}\mathcal{A}}} w_{(Z)}^{3} \right), \tag{A4}$$

$$\sqrt{\frac{\Sigma\Delta}{-g_{tt}\mathcal{A}}}\Gamma_{(Z)} - \Gamma_{(S)} = \frac{a\mathcal{B}\sin\theta}{\sqrt{-g_{tt}\Sigma\mathcal{A}}}\Gamma_{(Z)}w_{(Z)}^{3}, \quad (A5)$$

$$\Gamma_{(Z)} - \sqrt{\frac{\Sigma \Delta}{-g_{tt} \mathcal{A}}} \Gamma_{(S)} = \frac{a \mathcal{B} \sin \theta}{\sqrt{-g_{tt} \Sigma \mathcal{A}}} \Gamma_{(S)} w_{(S)}^{3} , \quad (A6)$$

$$-\frac{1+\Gamma_{(Z)}}{1+\Gamma_{(S)}} \left[\left(1 - \sqrt{\frac{\Sigma \Delta}{-g_{tt} \mathcal{A}}} \right) \frac{\Gamma_{(Z)} w_{(Z)}^{3}}{1+\Gamma_{(Z)}} + \frac{a \mathcal{B} \sin \theta}{\sqrt{-g_{tt} \Sigma \mathcal{A}}} \right]$$

$$= \left(1 - \sqrt{\frac{\Sigma \Delta}{-g_{tt} \mathcal{A}}} \right) \frac{\Gamma_{(S)} w_{(S)}^{3}}{1+\Gamma_{(S)}} - \frac{a \mathcal{B} \sin \theta}{\sqrt{-g_{tt} \Sigma \mathcal{A}}}. \tag{A7}$$

⁹ The influence of the spin magnitude for the orbit and thus for the precessional angular velocity is considered on Figs. 1 and 2. For small spins we obtain an almost geodesic trajectory as a benchmark since in this case the right hand sides of the MPD equations are negligible.

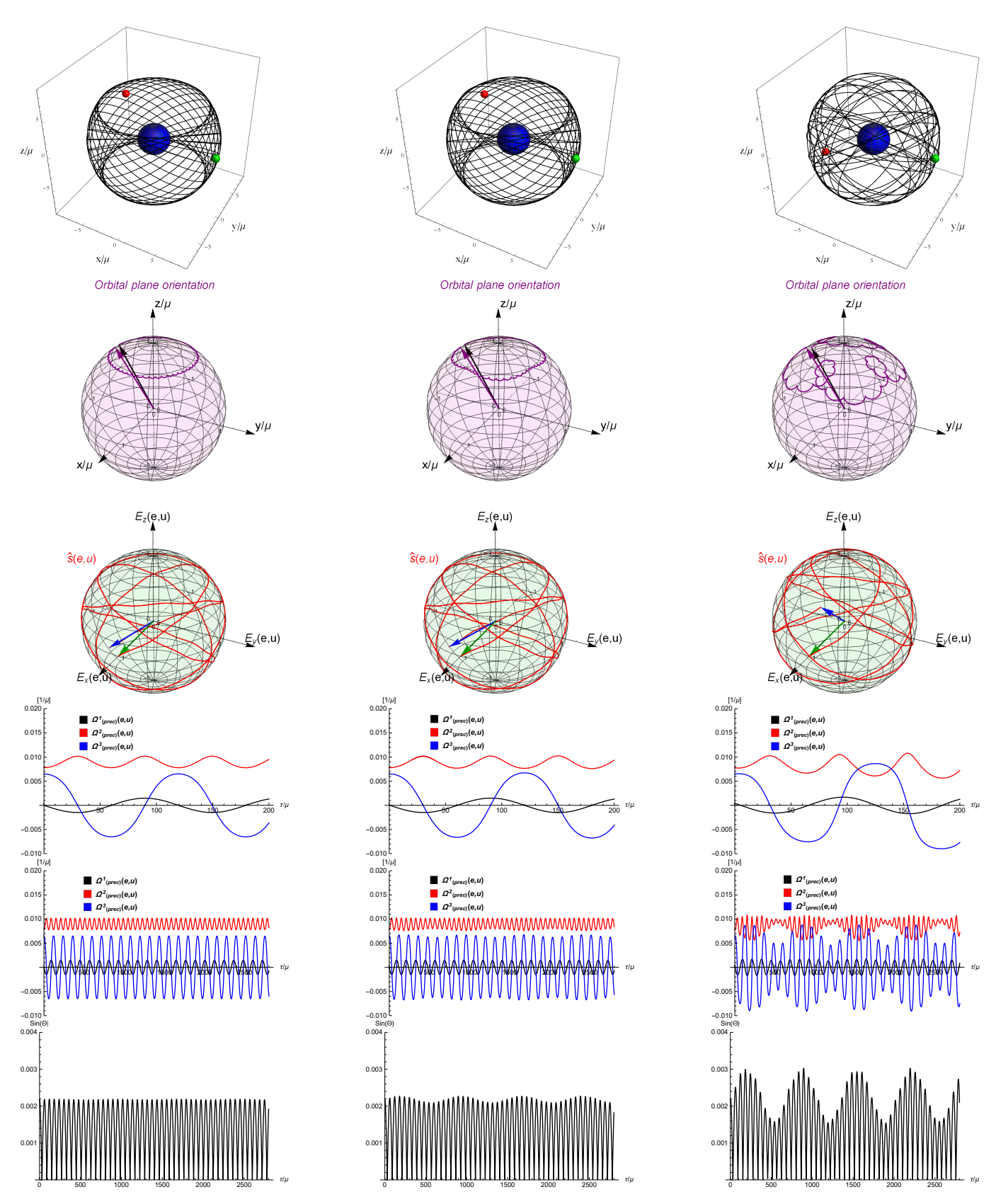


Figure 1: (color online). The evolution of spinning body moving on spherical-like orbits around the Kerr black hole with $a=0.5\mu$. From left to right the magnitude of the body's spin increases as $|s|/\mu m=0.01$, 0.1 and 0.9. The rows represent the following: 1. the orbit in coordinate space $(x/\mu,y/\mu,z/\mu)$ (the ergosphere of the central black hole is marked by blue and the initial and the final positions of the spinning body are denoted by green and red dots, respectively,), 2. the instantaneous orbital plane orientation l^i (initial and final directions are marked by purple and black arrows, respectively), 3. unit spin vector in the boosted SO comoving Cartesian-like frame E_i (e, u) (initial and final spin directions are marked by green and blue arrows, respectively), 4. and 5. $\Omega^{\alpha}_{(prec)}$ (e, u) on shorter and longer timescales, respectively, 6. sin Θ . The initial place of the body is $r(0)=8\mu$, $\theta(0)=\pi/2$ and $\phi(0)=0$. In the comparison of evolutions represented in the FMP and TD SSCs, the same dimensionless spin vector is chosen, i.e. $s^a/m=S^a/M$. The direction of the initial spin vector is given by $\theta^{(S)}$ (0) = $\pi/2$ and $\phi^{(S)}$ (0) in the boosted SO frame (resulting in S^r (0) $/|S|=s^r$ (0) /|s|=0.8682, μ (0) $/|S|=\mu s^\theta$ (0) /|s|=0 and μ (0) $/|S|=\mu s^\phi$ (0) /|S|=0 in Boyer-Lindquist coordinates). The four momentum $p^a_{(TD)}/M$ is chosen for the TD SSC as $p^a_{(TD)}(0)/M$ (0) = 0, μ (16). This four velocity is identified with the initial centroid four velocity in the FMP SSC as $u^a_{(FMP)}=u^a_{(TD)}$ and the initial four momentum $p^a_{(FMP)}/m$ is derived from Eq. (100).

Appendix B: The relation between the frames $E_{\alpha}\left(e,U\right)$ and $E_{\alpha}\left(f,U\right)$

The frame vectors $E_{\alpha}(e, U)$ derived from the SO's frame are the following linear combination of $E_{\alpha}(f, U)$:

$$E_{1}(e,U) = E_{1}(f,U) + \frac{\Gamma_{(Z)}w_{(Z)}^{1}}{1 + \Gamma_{(S)}} \left[\frac{a\mathcal{B}\sin\theta}{\sqrt{-g_{tt}\Sigma\mathcal{A}}} E_{3}(f,U) + \left(1 - \sqrt{\frac{\Sigma\Delta}{-g_{tt}\mathcal{A}}}\right) \frac{\Gamma_{(Z)}\mathbf{w}_{(Z)}}{1 + \Gamma_{(Z)}} \right],$$

$$\begin{split} E_{\mathbf{2}}\left(e,U\right) \; = \; E_{\mathbf{2}}\left(f,U\right) + \frac{\Gamma_{(Z)}w_{(Z)}^{2}}{1 + \Gamma_{(S)}} \left[\frac{a\mathcal{B}\sin\theta}{\sqrt{-g_{tt}\Sigma\mathcal{A}}} E_{\mathbf{3}}\left(f,U\right) \right. \\ \left. + \left(1 - \sqrt{\frac{\Sigma\Delta}{-g_{tt}\mathcal{A}}}\right) \frac{\Gamma_{(Z)}\mathbf{w}_{(Z)}}{1 + \Gamma_{(Z)}} \right] \; , \end{split}$$

$$E_{3}(e,U) = \left(\sqrt{\frac{\Sigma\Delta}{-g_{tt}\mathcal{A}}} + \Gamma_{(Z)}\right) \frac{E_{3}(f,U)}{1 + \Gamma_{(S)}} - \frac{\Gamma_{(Z)}\mathbf{w}_{(Z)}}{1 + \Gamma_{(S)}}$$

$$\times \left[\left(1 - \sqrt{\frac{\Sigma\Delta}{-g_{tt}\mathcal{A}}}\right) \frac{\Gamma_{(Z)}w_{(Z)}^{3}}{1 + \Gamma_{(Z)}} + \frac{a\mathcal{B}\sin\theta}{\sqrt{-g_{tt}\Sigma\mathcal{A}}}\right]$$
(B1)

The inverse relations are

$$E_{1}(f,U) = E_{1}(e,U) - \frac{\Gamma_{(S)}w_{(S)}^{1}}{1 + \Gamma_{(Z)}} \left[\frac{a\mathcal{B}\sin\theta}{\sqrt{-g_{tt}\Sigma\mathcal{A}}} E_{3}(e,U) - \left(1 - \sqrt{\frac{\Sigma\Delta}{-g_{tt}\mathcal{A}}}\right) \frac{\Gamma_{(S)}\mathbf{w}_{(S)}}{1 + \Gamma_{(S)}} \right],$$

$$\begin{split} E_{\mathbf{2}}\left(f,U\right) \; = \; E_{\mathbf{2}}\left(e,U\right) - \frac{\Gamma_{(S)}w_{(S)}^{2}}{1 + \Gamma_{(Z)}} \left[\frac{a\mathcal{B}\sin\theta}{\sqrt{-g_{tt}\Sigma\mathcal{A}}} E_{\mathbf{3}}\left(e,U\right) \right. \\ \left. - \left(1 - \sqrt{\frac{\Sigma\Delta}{-g_{tt}\mathcal{A}}}\right) \frac{\Gamma_{(S)}\mathbf{w}_{(S)}}{1 + \Gamma_{(S)}} \right] \; , \end{split}$$

$$E_{\mathbf{3}}(f,U) = \left(\sqrt{\frac{\Sigma\Delta}{-g_{tt}\mathcal{A}}} + \Gamma_{(S)}\right) \frac{E_{\mathbf{3}}(e,U)}{1 + \Gamma_{(Z)}} - \frac{\Gamma_{(S)}\mathbf{w}_{(S)}}{1 + \Gamma_{(Z)}}$$
$$\times \left[\left(1 - \sqrt{\frac{\Sigma\Delta}{-g_{tt}\mathcal{A}}}\right) \frac{\Gamma_{(S)}w_{(S)}^{\mathbf{3}}}{1 + \Gamma_{(S)}} - \frac{a\mathcal{B}\sin\theta}{\sqrt{-g_{tt}\Sigma\mathcal{A}}}\right] .(B2)$$

The frame components of any vector field

$$\mathbf{V} = \overset{(e)}{V^{\alpha}} E_{\alpha} (e) = \overset{(f)}{V^{\alpha}} E_{\alpha} (f) , \qquad (B3)$$

obey the following transformation rule

$$V^{1} = V^{1} + \left[\left(1 - \sqrt{\frac{\Sigma \Delta}{-g_{tt} A}} \right) \frac{\Gamma_{(Z)} \mathbf{w}_{(Z)} \cdot \mathbf{V}}{1 + \Gamma_{(Z)}} + \frac{a \mathcal{B} \sin \theta}{\sqrt{-g_{tt} \Sigma A}} V^{3} \right] \frac{\Gamma_{(Z)} \mathbf{w}_{(Z)}^{1}}{1 + \Gamma_{(S)}} ,$$

$$V^{2} = V^{2} + \left[\left(1 - \sqrt{\frac{\Sigma \Delta}{-g_{tt} A}} \right) \frac{\Gamma_{(Z)} \mathbf{w}_{(Z)} \cdot \mathbf{V}}{1 + \Gamma_{(Z)}} + \frac{a \mathcal{B} \sin \theta}{\sqrt{-g_{tt} \Sigma A}} V^{3} \right] \frac{\Gamma_{(Z)} \mathbf{w}_{(Z)}^{2}}{1 + \Gamma_{(S)}} ,$$

$$V^{\mathbf{3}} = \left(\sqrt{\frac{\Sigma\Delta}{-g_{tt}\mathcal{A}}} + \Gamma_{(Z)}\right) \frac{V^{\mathbf{3}}}{1 + \Gamma_{(S)}} - \frac{\Gamma_{(Z)}\mathbf{w}_{(Z)} \cdot \mathbf{V}}{1 + \Gamma_{(S)}}$$
$$\times \left[\frac{a\mathcal{B}\sin\theta}{\sqrt{-g_{tt}\Sigma\mathcal{A}}} + \left(1 - \sqrt{\frac{\Sigma\Delta}{-g_{tt}\mathcal{A}}}\right) \frac{\Gamma_{(Z)}\mathbf{w}_{(Z)}^{\mathbf{3}}}{1 + \Gamma_{(Z)}}\right], \quad (B4)$$

with $\mathbf{w}_{(Z)}$ introduced in Eq. (45).

The inverse relations are

$$\begin{array}{ll} \boldsymbol{V^1} &=& \boldsymbol{V^1} + \left[\left(1 - \sqrt{\frac{\Sigma \Delta}{-g_{tt} \mathcal{A}}} \right) \frac{\Gamma_{(S)} \mathbf{w}_{(S)} \cdot \mathbf{V}}{1 + \Gamma_{(S)}} \right. \\ & \left. - \frac{a \mathcal{B} \sin \theta}{\sqrt{-g_{tt} \Sigma \mathcal{A}}} \boldsymbol{V^3} \right] \frac{\Gamma_{(S)} \boldsymbol{w}_{(S)}^1}{1 + \Gamma_{(Z)}} \; , \end{array}$$

$$\begin{split} \boldsymbol{V^2} &= \boldsymbol{V^2} + \left[\left(1 - \sqrt{\frac{\Sigma \Delta}{-g_{tt} \mathcal{A}}} \right) \frac{\Gamma_{(S)} \mathbf{w}_{(S)} \cdot \mathbf{V}}{1 + \Gamma_{(S)}} \right. \\ &\left. - \frac{a \mathcal{B} \sin \theta}{\sqrt{-g_{tt} \Sigma \mathcal{A}}} \boldsymbol{V^3} \right] \frac{\Gamma_{(S)} \boldsymbol{w}_{(S)}^2}{1 + \Gamma_{(Z)}} \;, \end{split}$$

$$V^{3} = \left(\sqrt{\frac{\Sigma\Delta}{-g_{tt}\mathcal{A}}} + \Gamma_{(S)}\right) \frac{V^{3}}{1 + \Gamma_{(Z)}} + \frac{\Gamma_{(S)}\mathbf{w}_{(S)} \cdot \mathbf{V}}{1 + \Gamma_{(Z)}}$$
$$\times \left[\frac{a\mathcal{B}\sin\theta}{\sqrt{-g_{tt}\Sigma\mathcal{A}}} - \left(1 - \sqrt{\frac{\Sigma\Delta}{-g_{tt}\mathcal{A}}}\right) \frac{\Gamma_{(S)}w_{(S)}^{3}}{1 + \Gamma_{(S)}}\right], \quad (B5)$$

with $\mathbf{w}_{(S)}$ introduced in Eq. (41).

[1] B. P. Abbott et al. (LIGO Scientific, Virgo), Observation of Gravitational Waves from a Binary Black

Hole Merger, Phys. Rev. Lett. 116, 061102 (2016).

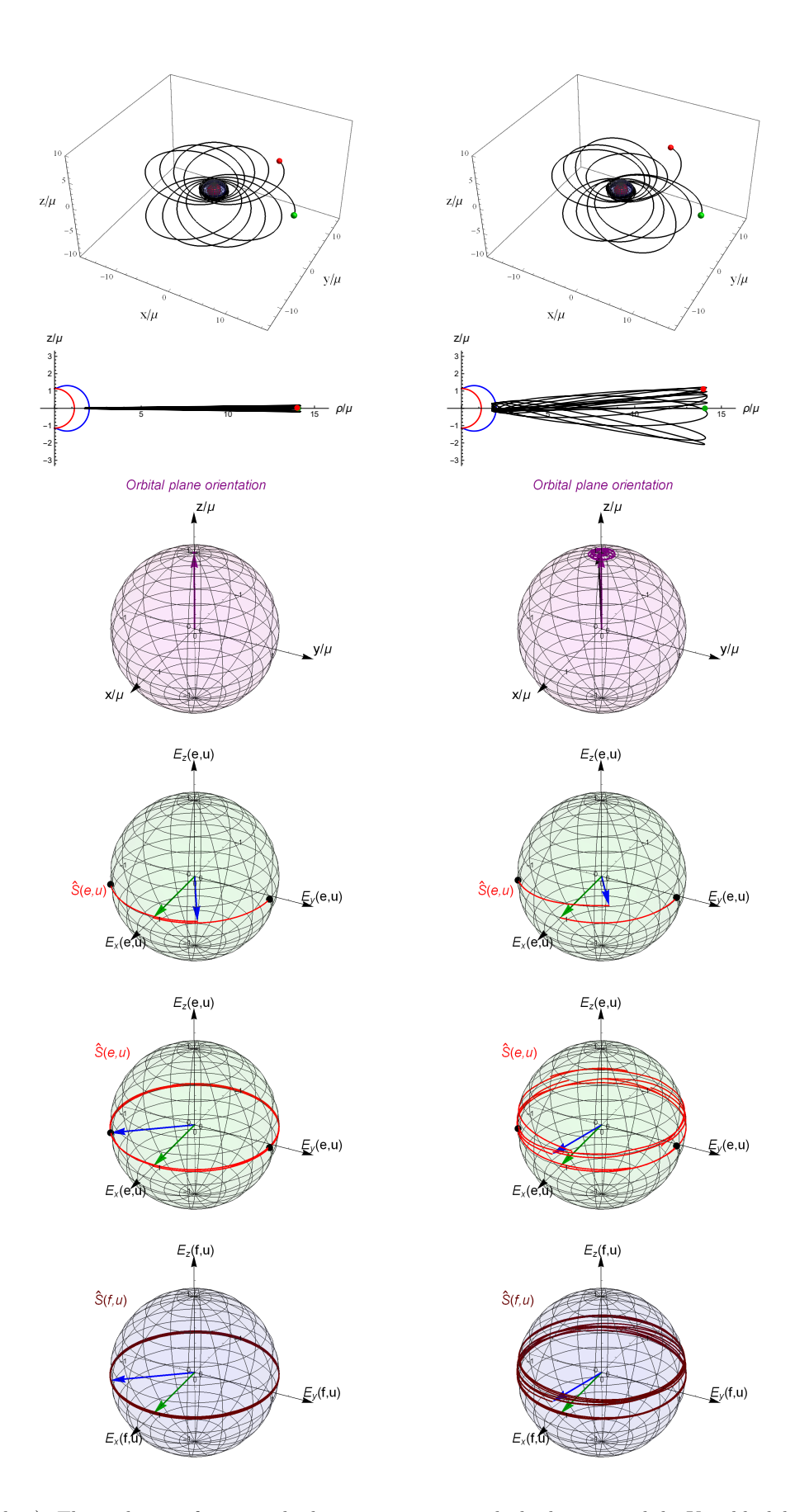


Figure 2: (color online). The evolution of spinning body moving on zoom-whirl orbits around the Kerr black hole with $a=0.99\mu$. The magnitudes of the body's spin are $|S|/\mu M=0.01$ (left panel) and 0.1 (right panel). The rows represent the following: 1. the orbit in coordinate space $(x/\mu,y/\mu,z/\mu)$ (outer and inner bounds of the ergosphere of the central black hole is marked by blue and red surfaces, respectively, and initial and final positions of the spinning body are denoted by green and red dots, respectively), 2. the orbit in the coordinate space $\rho/\mu = r\sin\theta/\mu$ and $z/\mu = r\cos\theta/\mu$ with marked initial and final positions and bounds of the ergosphere, 3. the instantaneous orbital plane orientation l^i (initial and final directions are marked by purple and black arrows, respectively), 4. and 5. unit spin vector in the boosted SO Cartesian-like comoving frame $E_i(e,u)$ on a shorter timescale and on the total timescale, respectively, and 6. unit spin vector in the boosted ZAMO Cartesian-like comoving frame $E_i(f,u)$ only on the total timescale (initial and final spin directions are marked by green and blue arrows, respectively). The initial data set: t(0) = 0, $r(0) = 14.05\mu$, $\theta(0) = \pi/2$, $\phi(0) = 0$, $p^r(0)/M = -0.03$, $\mu p^\theta(0)/M = 0$, $\mu p^\phi(0)/M = 0.012$, $\theta^{(S)}(0) = \pi/2$ and $\phi^{(S)}(0) = 0$ (the spatial Boyer-Lindquist coordinate components are $S^r(0)/|S| = 0.9293$, $\mu S^\theta(0)/|S| = 0$ and $\mu S^\phi(0)/|S| = -0.0002$).

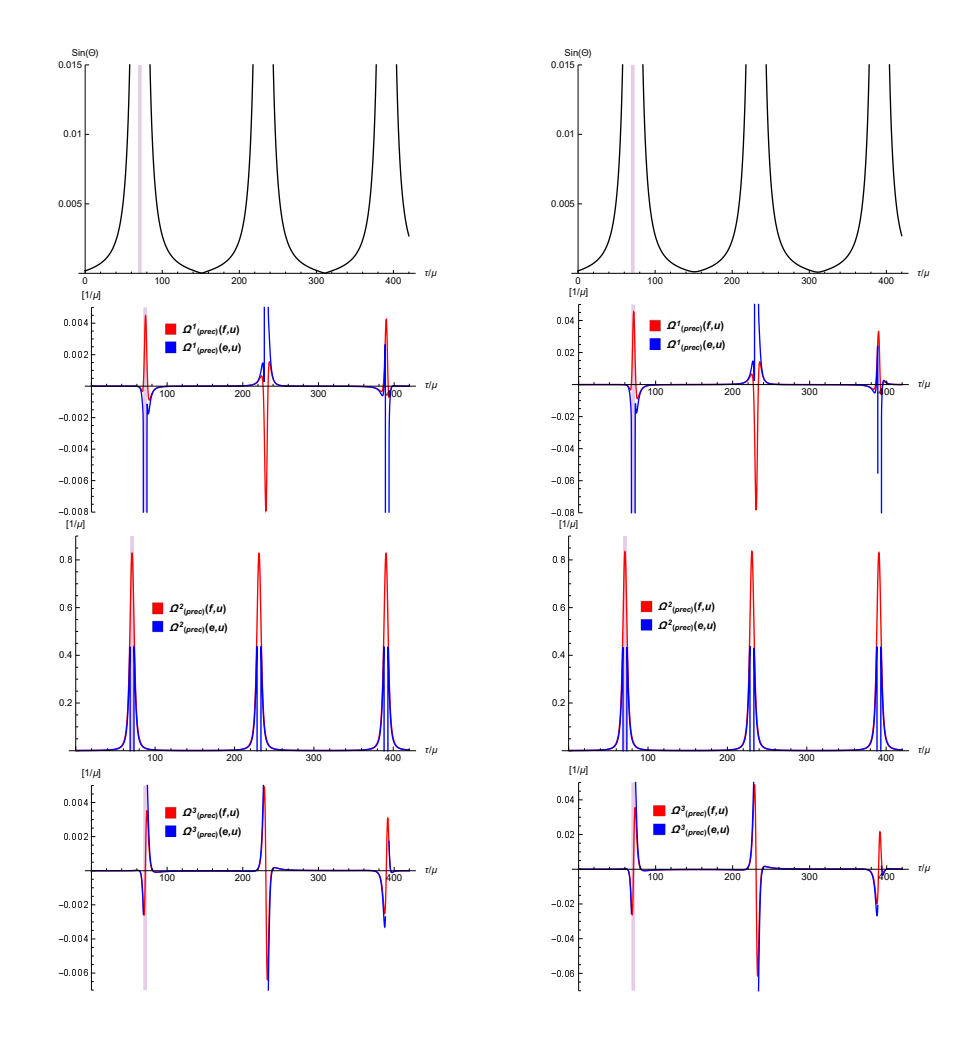


Figure 3: (color online). The left and right columns belong to the same evolution which are shown on Fig. 2. The first row shows $\sin \Theta$. On the next three rows we present the evolutions of the spherical triad components of the spin precessional angular velocities $\Omega^{\alpha}_{(prec)}(e,u)$ and $\Omega^{\alpha}_{(prec)}(f,u)$.

[arXiv:1602.03837]

- B. P. Abbott et al. (LIGO Scientific, Virgo), GW151226:
 Observation of Gravitational Waves from a 22-Solar-Mass Binary Black Hole Coalescence, Phys. Rev. Lett. 116, 241103 (2016). [arXiv:1606.04855]
- [3] B. P. Abbott et al. (LIGO Scientific, Virgo), GW170104: Observation of a 50-Solar-Mass Binary Black Hole Coalescence at Redshift 0.2, Phys. Rev. Lett. 118, 221101 (2017). [arXiv:1706.01812]
- [4] B. P. Abbott et al. (LIGO Scientific, Virgo), GW170814: A Three-Detector Observation of Gravitational Waves from a Binary Black Hole Coalescence, Phys. Rev. Lett. 119, 141101 (2017). [arXiv:1709.09660]
- [5] B. P. Abbott et al. (LIGO Scientific, Virgo), GW170817:
 Observation of Gravitational Waves from a Binary Neutron Star Inspiral, Phys. Rev. Lett. 119, 161101 (2017).
 [arXiv:1710.05832]
- [6] B. P. Abbott et al. (LIGO Scientific, Virgo), Gravitational Waves and Gamma-Rays from a Binary Neutron Star Merger: GW170817 and GRB 170817A, Astrophys. J. Lett. 848, L13 (2017). [arXiv:1710.05834]
- [7] B. P. Abbott et al. (LIGO Scientific, Virgo),

- GW170608: Observation of a 19 Solar-mass Binary Black Hole Coalescence, Astrophys. J. **851**, L35 (2017). [arXiv:1711.05578]
- [8] B. P. Abbott et al. (LIGO Scientific, Virgo), GWTC-1: A Gravitational-Wave Transient Catalog of Compact Binary Mergers Observed by LIGO and Virgo during the First and Second Observing Runs, (2018). [arXiv:1811.12907]
- [9] C. Kimball, C. P. L. Berry and V. Kalogera, What GW170729's exceptional mass and spin tells us about its family tree, (2019). [arXiv:1903.07813]
- [10] E. Kun, K. É. Gabányi, M. Karouzos, S. Britzen, L. Á. Gergely, A spinning supermassive black hole binary model consistent with VLBI observations of the S5 1928+738 jet, Mon. Not. Royal Astron. Soc. 445 (2), 1370 (2014). [arXiv:1402.2644]
- [11] B. M. Barker, R. F. O'Connell, Derivation of the Equations of Motion of a Gyroscope from the Quantum Theory of Gravitation, Phys. Rev. D 2, 1428 (1970).
- [12] B. M. Barker, R. F. O'Connell, Gravitational two-body problem with arbitrary masses, spins, and quadrupole moments, Phys. Rev. D 12, 329 (1975).

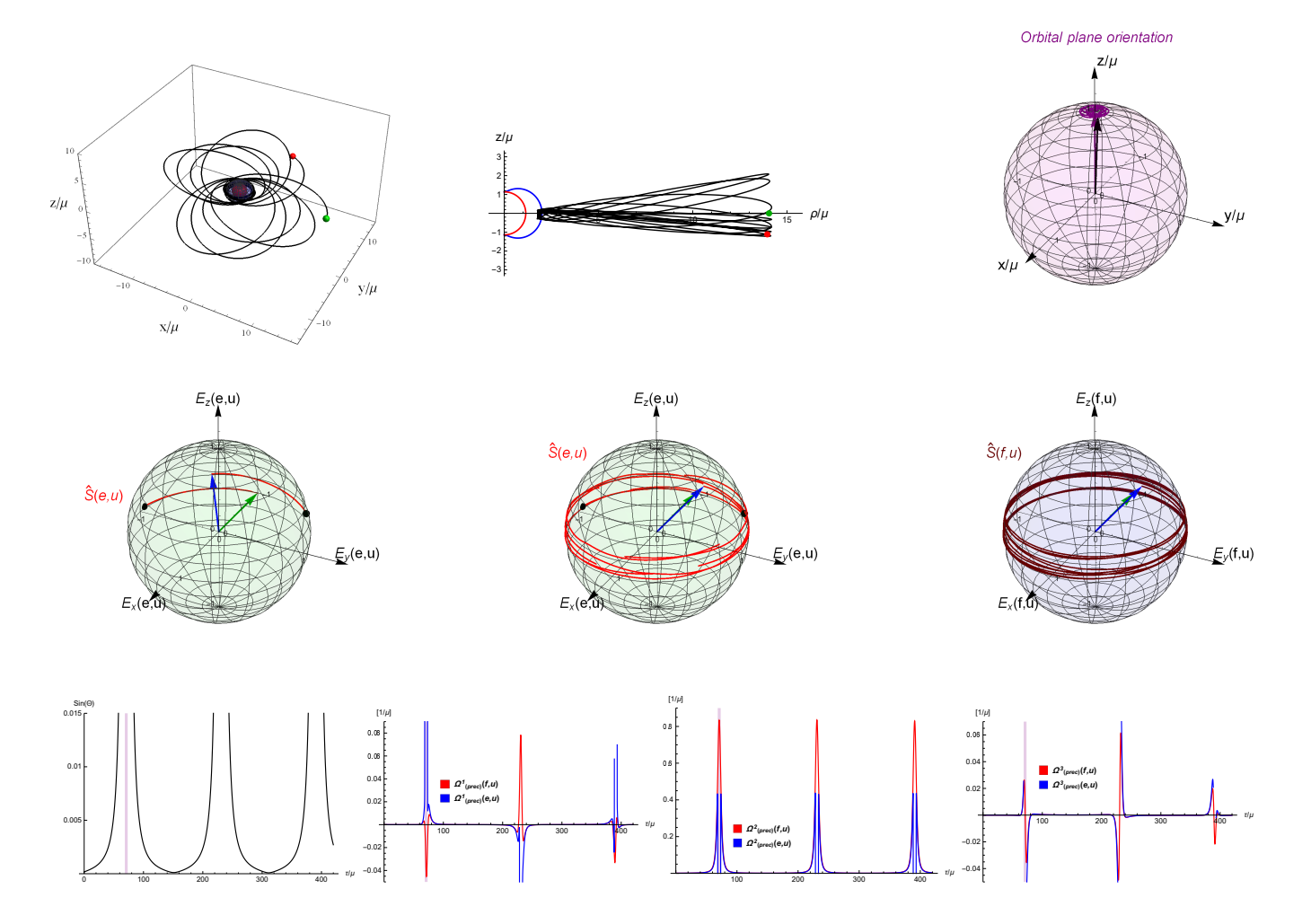


Figure 4: (color online). The initial direction of the spin vector is opposite with respect to the previous case presented on Figs. 2 and 3. The other initial data set is the same as on the second columns of Figs. 2 and 3 (e.g. $|S|/\mu M=0.1$). The spatial Boyer-Lindquist coordinate components of the initial spin vector is $S^r(0)/|S|=-0.9293$, $\mu S^\theta(0)/|S|=0$ and $\mu S^\phi(0)/|S|=0.0002$. From the upper left panel to the lower right, the pictures represent the followings: 1. the orbit in coordinate space $(x/\mu,y/\mu,z/\mu)$ (outer and inner bounds of the ergosphere of the central black hole is marked by blue and red surfaces, respectively, and the initial and the final positions of the spinning body are denoted by green and red dots, respectively), 2. the orbit in coordinate space $\rho/\mu = r\sin\theta/\mu$ and $z/\mu = r\cos\theta/\mu$ with marked initial and final positions and bounds of ergosphere, 3. the instantaneous orbital plane l^i (initial and final directions are marked by purple and black arrows, respectively), 4. and 5. unit spin vector in the boosted SO Cartesian-like comoving frame $E_i(e,u)$ on a shorter timescale and on the total timescale, respectively, and 6. unit spin vector in the boosted ZAMO Cartesian-like comoving frame $E_i(f,u)$ only on the total timescale (initial and final spin directions are marked by green and blue arrows, respectively), 7. $\sin \Theta$, 8.-10. the evolutions of the spherical triad components of the spin precessional angular velocities $\Omega^\alpha_{(prec)}(e,u)$ and $\Omega^\alpha_{(prec)}(f,u)$.

- [13] L. E. Kidder, Coalescing binary systems of compact objects to $(post)^{5/2}$ -Newtonian order. V. Spin effects, Phys. Rev. D **52**, 821 (1995).
- [14] E. Poisson, Gravitational waves from inspiraling compact binaries: The quadrupole-moment term, Phys. Rev. D 57, 5287 (1998).
- [15] N. Wex, The second post-Newtonian motion of compact binary-star systems with spin, Class. Quantum Grav 12, 983 (1995).
- [16] C. Königsdörffer and A. Gopakumar, Post-Newtonian accurate parametric solution to the dynamics of spinning compact binaries in eccentric orbits: The leading order spin-orbit interaction, Phys. Rev. D 71, 024039

- (2005).
- [17] Z. Keresztes, B. Mikóczi and L. Á. Gergely, Kepler equation for inspiralling compact binaries, Phys. Rev. D 71, 124043 (2005).
- [18] C. Königsdörffer and A. Gopakumar, Parametric derivation of the observable relativistic periastron advance for binary pulsars, Phys. Rev. D 73, 044011 (2006).
- [19] É. Racine, Analysis of spin precession in binary black hole systems including quadrupole-monopole interaction, Phys. Rev. D 78, 044021 (2008).
- [20] M. Kesden, D. Gerosa, R. O'Shaughnessy, E. Berti, and U. Sperhake, Effective Potentials and Morpholog-

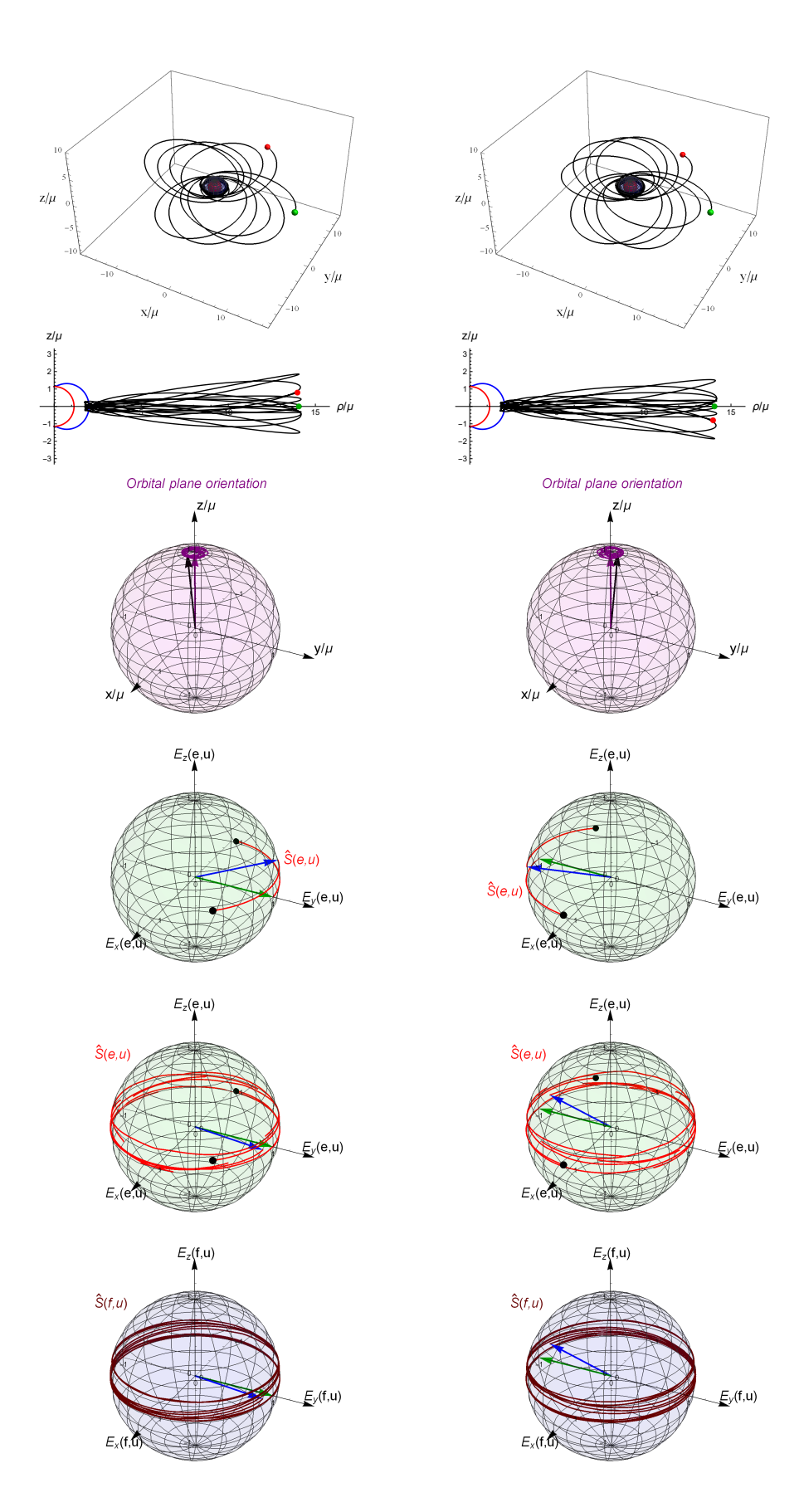


Figure 5: (color online). The same as on the last column of Figs. 2, but the initial direction of the spin vector is rotated by $\pi/2$ (left column) and by $-\pi/2$ (right column). (The spatial Boyer-Lindquist coordinate components of the spin vector are $S^{r}(0)/|S| = -0.0025$ (left column), 0.0025 (right column), $\mu S^{\theta}(0)/|S| = 0$ (both left and right columns) and $\mu S^{\phi}(0)/|S| = 0.0720$ (left column), -0.0720 (right column).

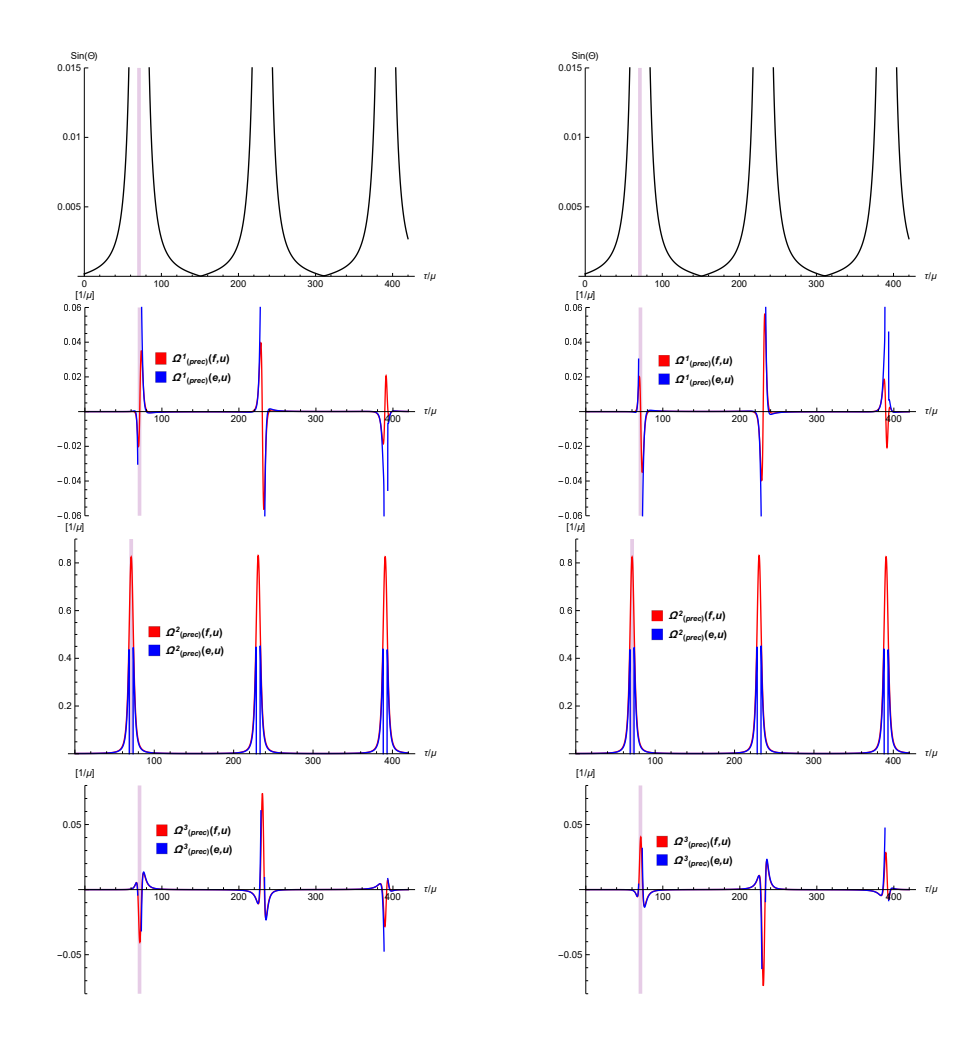


Figure 6: (color online). On the left and right columns the evolutions of $\sin \Theta$ and the spherical triad components of the spin precessional angular velocities are presented along those orbits which are shown in the left and right columns of Fig. 5, respectively.

- ical Transitions for Binary Black Hole Spin Precession, Phys. Rev. Lett. **114**, 081103 (2015). [arXiv:1411.0674]
- [21] T. A. Apostolatos, C. Cutler, G. J. Sussman, K. S. Thorne, Spin-induced orbital precession and its modulation of the gravitational waveforms from merging binaries, Phys. Rev. D 49, 6274 (1994).
- [22] J. D. Schnittman, Spin-Orbit Resonance and the Evolution of Compact Binary Systems, Phys. Rev. D 70, 124020 (2004). [arXiv:astro-ph/0409174]
- [23] L. Á. Gergely and P. L. Biermann, The spin-flip phenomenon in supermassive black hole binary mergers, Astrophys. J. 697, 1621 (2009). [arXiv:0704.1968]
- [24] C. O. Lousto, J. Healy, Flip-flopping binary black holes, Phys. Rev. Lett. 114, 141101 (2015). [arXiv:1410.3830]
- [25] D. Gerosa, A. Lima, E. Berti, U. Sperhake, M. Kesden and R. O'Shaughnessy, Wide precession: binary blackhole spins repeatedly oscillating from full alignment to full anti-alignment, (2018). [arXiv:1811.05979]
- [26] M. Mathisson, Neue Mechanik Materieller Systeme, Acta. Phys. Polon. 6, 163 (1937).
- [27] A. Papapetrou, Equations of Motion in General Relativity, Proc. Phys. Soc. 64, 57 (1951).
- [28] W. Dixon, A covariant multipole formalism for extended

- test bodies in general relativity, Nuovo Cim. **34**, 317 (1964).
- [29] W. G. Dixon, Dynamics of Extended Bodies in General Relativity. I. Momentum and Angular Momentum, Proc. R. Soc. London A, 314, 499 (1970).
- [30] W. G. Dixon, Extended Bodies in General Relativity: Their Description and Motion., in Isolated Gravitating Systems in General Relativity, Proceedings of the International School of Physics, Course LXVII, ed. by J. Ehlers (1979).
- [31] P. Amaro-Seoane et al., Laser Interferometer Space Antenna, arXiv:1702.00786 (2017).
- [32] C. Huwyler, E. K. Porter and P. Jetzer, Supermassive Black Hole Tests of General Relativity with eLISA, Phys. Rev. D 91, 024037 (2015).
- [33] J. N. Bahcall and R. A. Wolf, Star distribution around a black hole in a globular cluster. II. Unequal star masses, Astrophys. J. 216, 883 (1977).
- [34] I. Bartos, Z. Haiman, B. Kocsis, Sz. Márka, Gas Cloud G2 Can Illuminate the Black Hole Population Near the Galactic Center, Phys. Rev. Lett. 110, 221102 (2013).
- [35] C. J. Hailey, K. Mori, F. E. Bauer, M. E. Berkowitz, J. Hong, B. J. Hord, A density cusp of quiescent X-ray

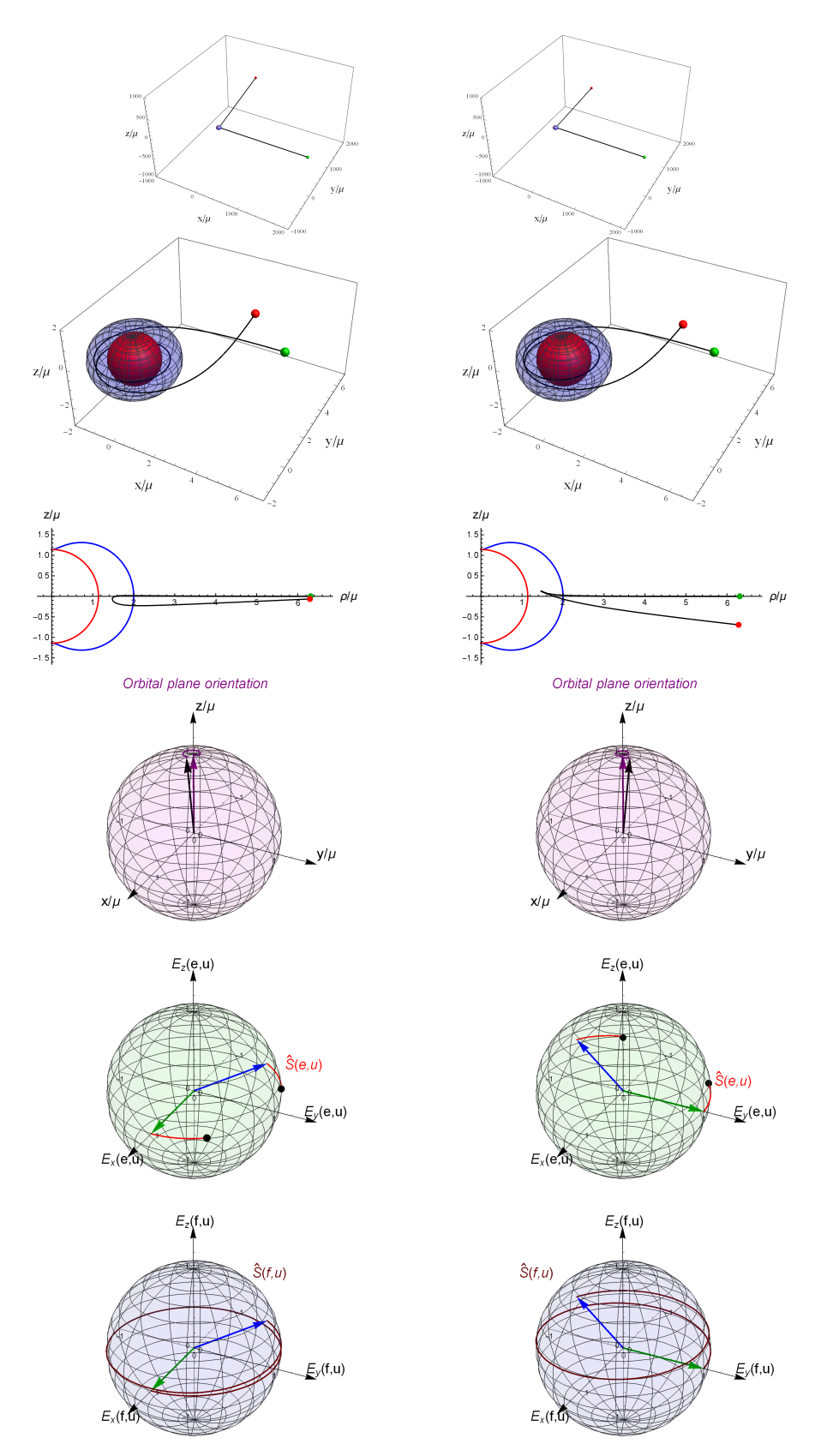


Figure 7: (color online). The evolutions of spinning body moving on unbound orbits around Kerr black hole with $a=0.99\mu$. The spin magnitude chosen as $|S|/\mu M=0.1$. The considered unbound orbits are shown in the first row. The near black hole parts of these orbits are represented in the second and third rows in $(x/\mu,y/\mu,z/\mu)$ and $(\rho/\mu,z/\mu)$ coordinates, respectively. The fourth, fifth and sixth rows give the evolutions of the instantaneous orbital plane and spin vector in the boosted ZAMO and SO frames, respectively. The initial spin direction is determined by $\phi^{(S)}(0)=\pi/2$ (left col.), 0 (right col.) and $\theta^{(S)}(0)=\pi/2$ (both cols.). The spatial Boyer-Lindquist coordinate components $[S^r(0),\mu S^\theta(0),\mu S^\phi(0)]/|S|$ of the spin vector are $[-0.0134,0,-3.1\times10^{-9}]$ and [-0.000006,0,0.000005] in the left and right columns, respectively. Additional initial data set is t(0)=0, $r(0)=2000\mu$, $\theta(0)=\pi/2$, $\phi(0)=0$, $p^r(0)/M=-0.9$, $\mu p^\phi(0)/M=8\times10^{-7}$ and $\mu p^\theta(0)/M=0$. The final locations $[t(\tau^*)/\mu,r(\tau^*)/\mu,\theta(\tau^*),\phi(\tau^*)]$ at $\tau^*=4433\mu$ are [6033.2,1999.7,1.527,14.24] (left col.) and [6033.3,1999.7,1.671,14.25] (right col.). The final values of the spatial Boyer-Lindquist coordinate components $[p^r(\tau^*),\mu p^\theta(\tau^*),\mu p^\phi(\tau^*)]/M$ of the four momentum are $[0.900002,-7.65\times10^{-8},8.00\times10^{-7}]$ (left col.) and $[0.900003,-3.48\times10^{-8},8.01\times10^{-7}]$ (right col.). The final values of the spatial Boyer-Lindquist components $[S^r(\tau^*),\mu S^\theta(\tau^*),\mu S^\phi(\tau^*)]/|S|$ of the spinvector are $[0.86,-2.9\times10^{-5},3.8\times10^{-4}]$ (left col.) and $[-1.11,-8.6\times10^{-5},2.7\times10^{-4}]$ (right col.). The final spin directions $[\theta^{(S)}(\tau^*),\phi^{(S)}(\tau^*)]$ in the boosted SO frame are determined by [1.48,-0.59] (left col.) and [1.31,1.09] (right col.). The angles $[\theta^{(I)}(\tau^*),\phi^{(I)}(\tau^*)]$ characterizing the final orbital plane orientations in coordinate space $(x/\mu,y/\mu,z/\mu)$ are [0.11,-0.33] (left col.) and [0.11,1.27] (right col.).

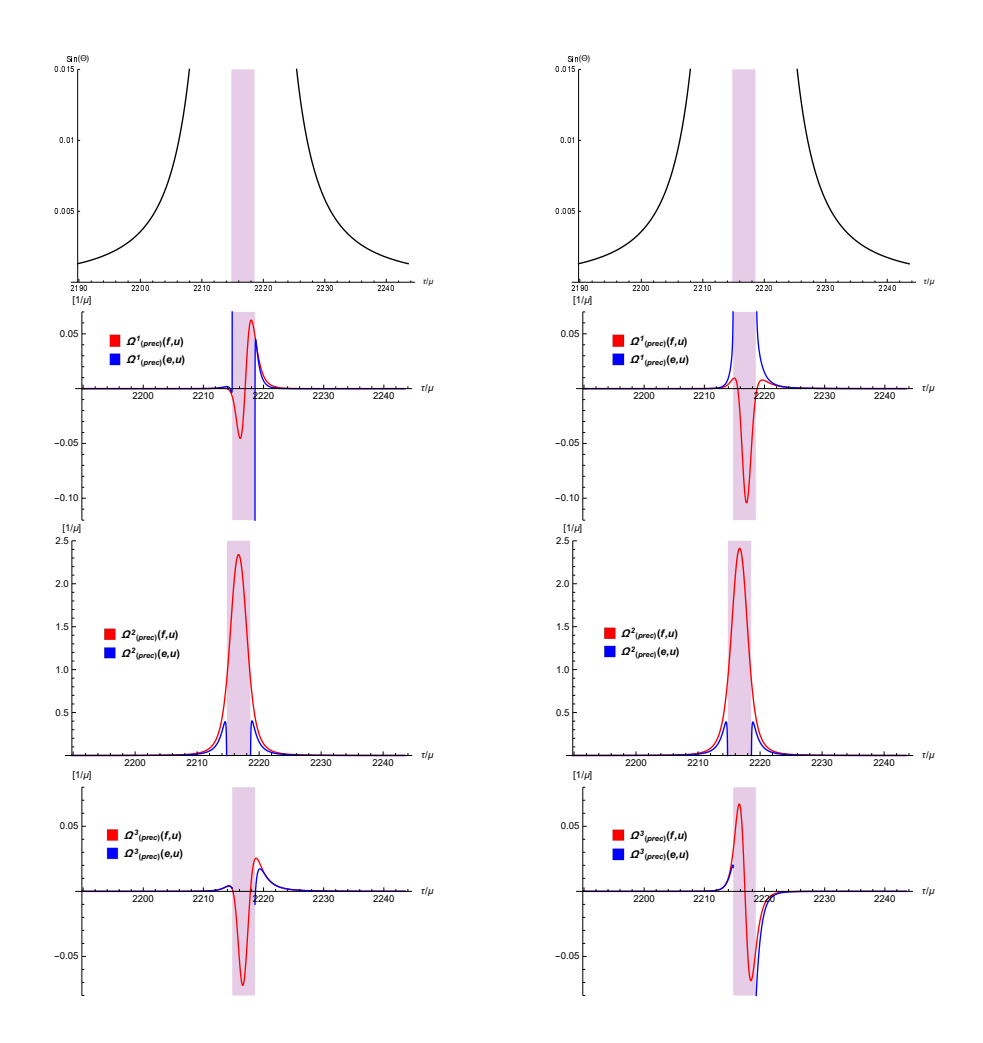


Figure 8: (color online). On the left and right columns the evolutions of $\sin\Theta$ and the spherical triad components of the spin precessional angular velocities are presented along those orbits which are shown in the left and right columns of Fig. 7, respectively.

- binaries in the central parsec of the Galaxy, Nature **556**, 70 (2018).
- [36] B. Mikóczi, Spin supplementary conditions for spinning compact binaries, Phys. Rev. D 95, 064023 (2017).
- [37] J. Frenkel, Die Elektrodynamik des rotierenden Elektrons, Z. Phys. 37, 243 (1926).
- [38] F. A. E. Pirani, On the Physical significance of the Riemann tensor, Acta Phys. Polon. 15, 389 (1956).
- [39] E. Corinaldesi and A. Papapetrou, Spinning Test-Particles in General Relativity. II, Proc. Roy. Soc. A 209, 259 (1951).
- [40] T. D. Newton and E. P. Wigner, Localized States for Elementary Systems, Rev. Mod. Phys. 21, 400 (1949).
- [41] M. H. L. Pryce, The Mass-Centre in the Restricted Theory of Relativity and Its Connexion with the Quantum Theory of Elementary Particles, Proc. Roy. Soc. Lond. A 195, 62 (1948).
- [42] W. M. Tulczyjew, Motion of multipole particles in general relativity theory, Acta Phys. Polon. 18, 393 (1959).
- [43] A. Ohashi, Multipole particle in relativity, Phys. Rev. D 68, 044009 (2003).
- [44] K. Kyrian and O. Semerák, Spinning test particles in a Kerr field - II, Mon. Not. Roy. Astron. Soc. 382, 1922

- (2007)
- [45] B. M. Barker & R. F. O'Connell, Nongeodesic moton in General Relativity, Gen. Rel. Grav. 5, 539 (1974).
- [46] O. Semerák, Spinning test particles in a Kerr field I, Mon. Not. Roy. Astron. Soc., 308, 863 (1999).
- [47] S. Suzuki and K. Maeda, Innermost Stable Circular Orbit of a Spinning Particle in Kerr Spacetime, Phys. Rev. D 58, 023005 (1998).
- [48] M. D. Hartl, A survey of spinning test particle orbits in Kerr spacetime, Phys. Rev. D 67, 104023 (2003).
- [49] M. D. Hartl, Dynamics of spinning test particles in Kerr spacetime, Phys. Rev. D, 67, 024005 (2003).
- [50] W.-B. Han and R. Cheng, Dynamics of extended bodies with spin-induced quadrupole in Kerr spacetime: generic orbits, Gen. Relativ. Gravit. 49, 48 (2017).
- [51] B. Mashhoon and D. Singh, Dynamics of extended spinning masses in a gravitational field, Phys. Rev. D 74, 124006 (2006).
- [52] D. Bini, P. Fortini, A. Geralico and A. Ortolan, Quadrupole effects on the motion of extended bodies in Kerr spacetime Class. Quant. Grav. 25, 125007 (2008).
- [53] D. Bini and A. Geralico, Spin-geodesic deviations in the Kerr spacetime, Phys. Rev. D 84, 104012 (2011).

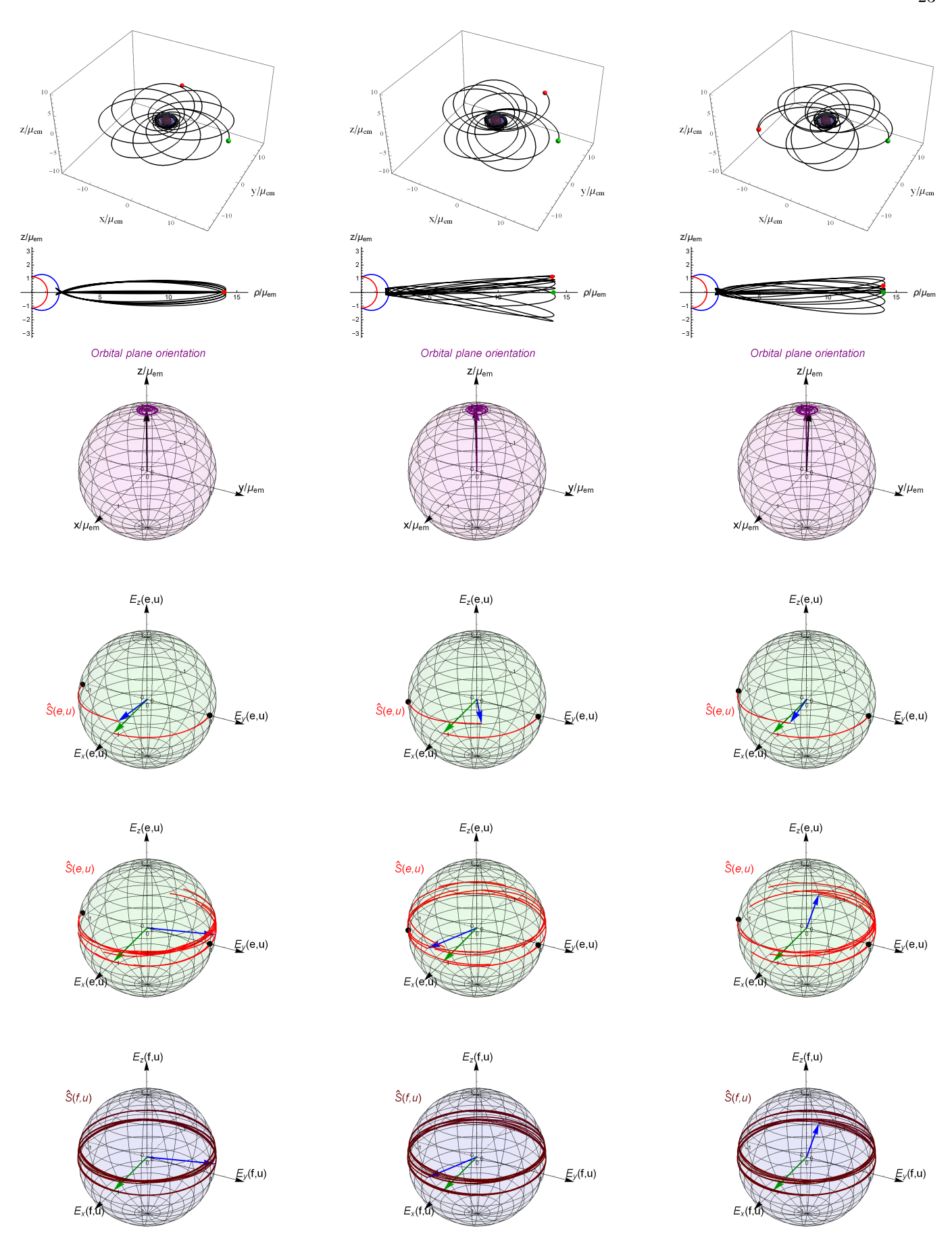


Figure 9: (color online). Zoom-whirl orbits are represented around regular, rotating black holes with $\gamma=3$ and $a=0.99\mu_{em}$. The first column shows the orbit around a Bardeen-like black hole ($\nu=2$) while the middle and the last around a Hayward-like black hole ($\nu=3$). The parameter q is 0.081 in the first two columns while 0.216 in third one. Applying the notation change $\mu\to\mu_{em}$, the initial values are chosen the same as in the second column of Fig. 2.

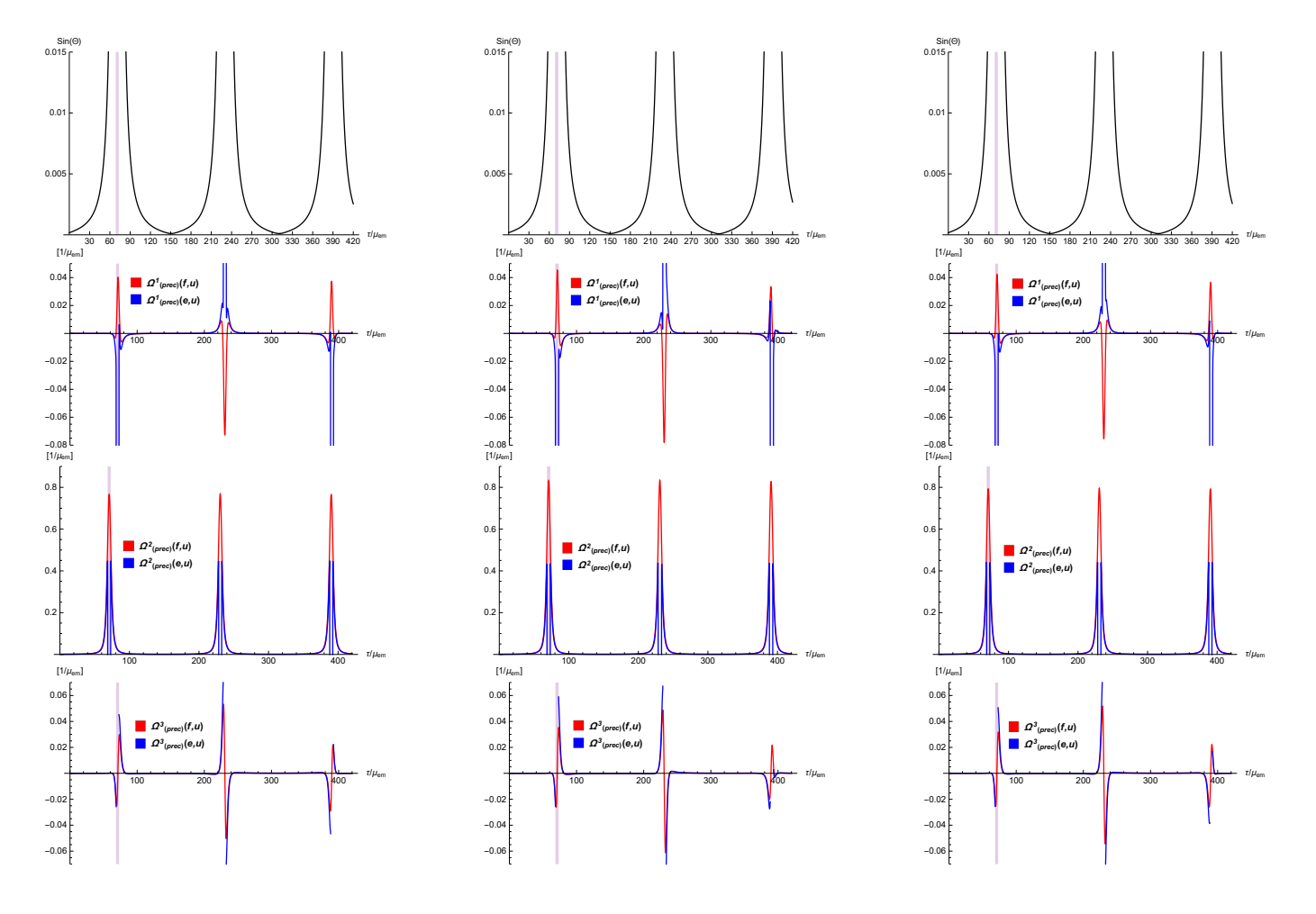


Figure 10: (color online). The evolutions of $\sin \Theta$ and the frame components of the spin precessional velocities are shown. The columns from left to right belong to the same evolutions which were presented on Fig. 9, respectively.

- [54] R. Plyatsko and M. Fenyk, Highly relativistic circular orbits of spinning particle in the Kerr field, Phys. Rev. D 87, 044019 (2013).
- [55] D. Bini and A. Geralico, Extended bodies in a Kerr spacetime: exploring the role of a general quadrupole tensor, Class. Quantum Grav. 31, 075024 (2014).
- [56] D. Bini, G. Faye and A. Geralico, Dynamics of extended bodies in a Kerr spacetime with spin-induced quadrupole tensor, Phys. Rev. D 92, 104003 (2015).
- [57] E. Hackmann, C. Lämmerzahl, Y. N. Obukhov, D. Puetzfeld, I. Schaffer, Motion of spinning test bodies in Kerr spacetime, Phys. Rev. D 90, 064035 (2014).
- [58] G. Lukes-Gerakopoulos, Time parameterizations and spin supplementary conditions of the Mathisson-Papapetrou-Dixon equations, Phys. Rev. D 96, 104023 (2017).
- [59] U. Ruangsri, S. J. Vigeland and S. A. Hughes, Gyroscopes orbiting black holes: A frequency-domain approach to precession and spin-curvature coupling for spinning bodies on generic Kerr orbits, Phys. Rev. D 94, 044008 (2016).
- [60] K. Glampedakis and D. Kennefick, Zoom and whirl: Eccentric equatorial orbits around spinning black holes and their evolution under gravitational radiation reaction,

- Phys. Rev. D 66 044002 (2002).
- [61] K. Glampedakis, S. A. Hughes, D. Kennefick, Approximating the inspiral of test bodies into Kerr black holes, Phys. Rev. D 66, 064005 (2002).
- [62] K. Glampedakis, Extreme Mass Ratio Inspirals: LISA's unique probe of black hole gravity, Class. Quant. Grav. 22, S605 (2005).
- [63] J. Levin and G. Perez-Giz, A periodic table for black hole orbits, Phys. Rev. D 77, 103005 (2008).
- [64] R. Grossman, J. Levin and G. Perez-Giz, The harmonic structure of generic Kerr orbits, Phys. Rev. D 85, 023012 (2012).
- [65] F. Pretorius and D. Khurana, Black hole mergers and unstable circular orbits, Class. Quantum Grav. 24, S83 (2007).
- [66] J. Healy, J. Levin and D. Shoemaker, Zoom-Whirl Orbits in Black Hole Binaries, Phys Rev. Let. 103, 131101 (2009).
- [67] U. Sperhake, V. Cardoso, F. Pretorius, E. Berti, T. Hinderer, N. Yunes, Cross Section, Final Spin, and Zoom-Whirl Behavior in High-Energy Black-Hole Collisions, Phys. Rev. Lett. 103, 131102 (2009).
- [68] R. Gold and B. Brügmann, Radiation from lowmomentum zoom-whirl orbits, Class. Quant. Grav. 27,

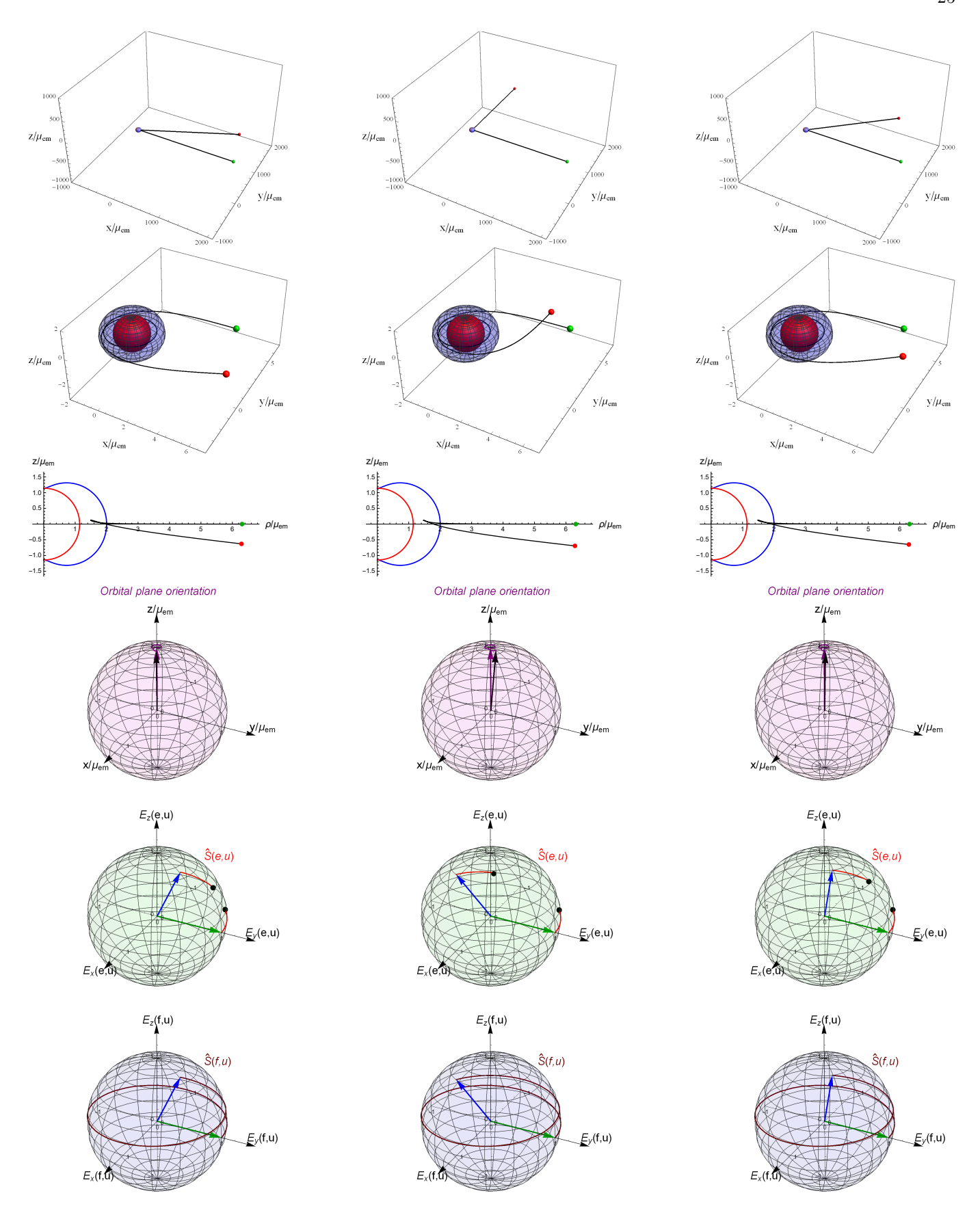


Figure 11: (color online). The evolutions along unbound orbits in cases of regular black holes $\gamma=3$ and $a=0.99\mu_{em}$. The parameter pair (ν,q) changes from left to right as (2,0.081), (3,0.081) and (3,0.216). With the notation change $\mu\to\mu_{em}$, the initial values are chosen the same as in the second column of Fig. 7. The final locations $[t(\tau^*)/\mu_{em}, r(\tau^*)/\mu_{em}, \theta(\tau^*), \phi(\tau^*)]$ at $\tau^*=4433\mu_{em}$ are [6030.6,1999.9,1.675,13.13] (1st col.), [6033.1,1999.7,1.672,14.20] (2nd col.) and [6031.3,1999.9,1.675,13.41] (3rd col.). The final values of the spatial Boyer-Lindquist coordinate components $[p^r(\tau^*),\mu_{em}p^\theta(\tau^*),\mu_{em}p^\phi(\tau^*)]/M$ of the four momentum are $[0.90003,-1.26\times10^{-8},8.03\times10^{-7}]$ (1st col.), $[0.900002,-3.38\times10^{-8},8.02\times10^{-7}]$ (2nd col.) and $[0.900003,-1.77\times10^{-8},8.02\times10^{-7}]$ (3rd col.). The final values of the spatial Boyer-Lindquist components $[S^r(\tau^*),\mu_{em}S^\theta(\tau^*),\mu_{em}S^\phi(\tau^*)]/|S|$ of the spinvector are $[-1.20,-7.6\times10^{-5},2.2\times10^{-4}]$ (1st col.), $[-1.11,-8.5\times10^{-5},2.7\times10^{-4}]$ (2nd col.) and $[-1.18,-7.9\times10^{-5},2.3\times10^{-4}]$ (3rd col.). The final spin directions $[\theta^{(S)}(\tau^*),\phi^{(S)}(\tau^*)]$ in the boosted SO frame are determined by [1.32,0.10] (1st col.), [1.31,1.04] (2nd col.) and [1.32,0.35] (3rd col.). The angles $[\theta^{(l)}(\tau^*),\phi^{(l)}(\tau^*)]$ characterizing the final orbital plane orientations in coordinate space $(x/\mu_{em},y/\mu_{em},z/\mu_{em})$ are [0.11,0.41] (1st col.), [0.11,1.23] (2nd col.) and [0.11,0.63] (3rd col.).

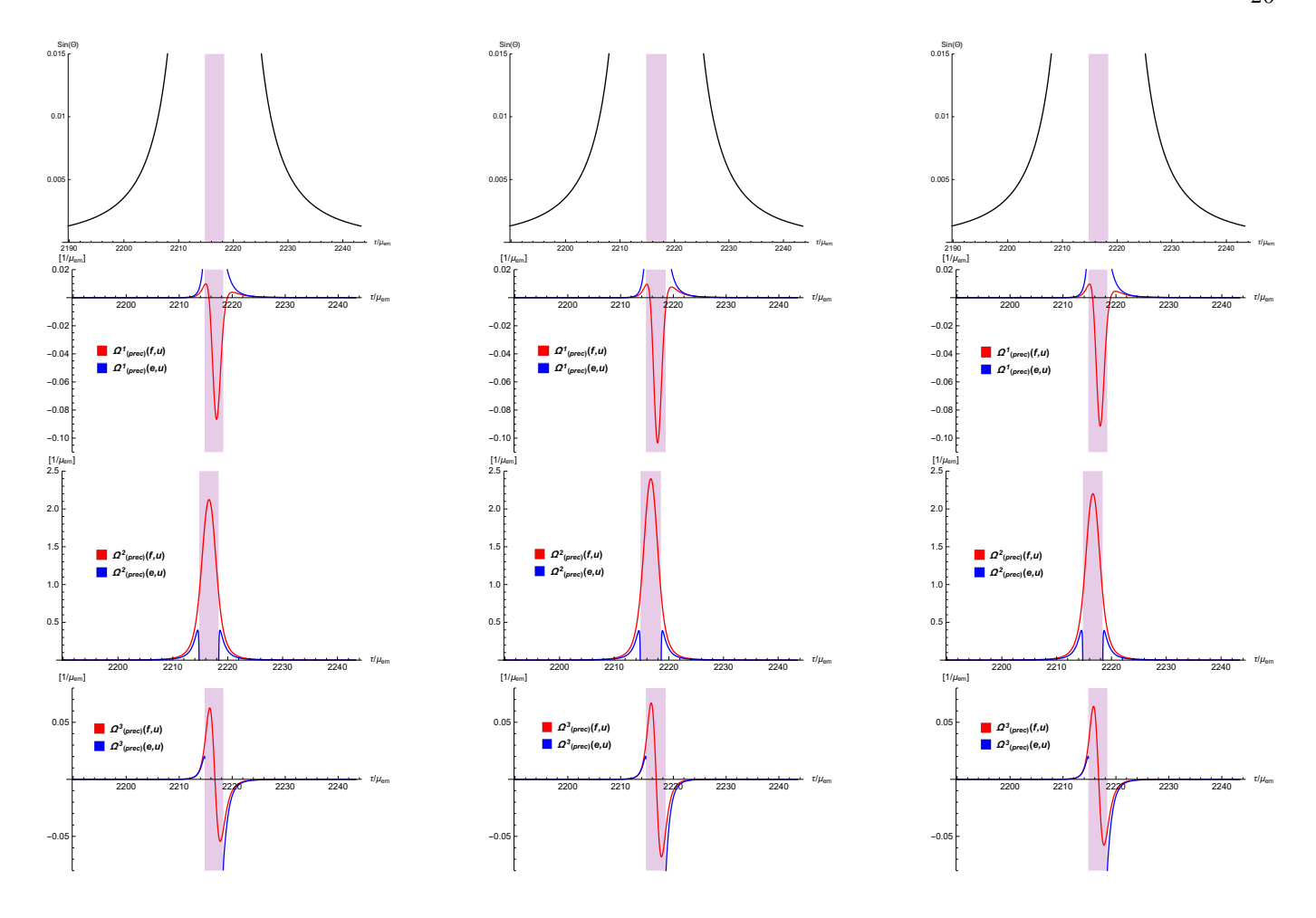


Figure 12: (color online). The evolution of $\sin \Theta$ and the frame components of the spin precessional velocities are shown. The columns from left to right belong to the same evolutions which were presented on Fig. 11, respectively.

- 084035 (2010).
- [69] R. Gold and B. Brügmann, Eccentric black hole mergers and zoom-whirl behavior from elliptic inspirals to hyperbolic encounters, Phys. Rev. D 88, 064051 (2013).
- [70] W. E. East, S. T. McWilliams, J. Levin, F. Pretorius, Observing complete gravitational wave signals from dynamical capture binaries, Phys. Rev. D 87, 043004 (2013).
- [71] J. Levin and R. Grossman, Dynamics of black hole pairs. I. Periodic tables, Phys. Rev. D 79, 043016 (2009).
- [72] R. Grossman and J. Levin, Dynamics of black hole pairs. II. Spherical orbits and the homoclinic limit of zoomwhirliness, Phys. Rev. D 79, 043017 (2009).
- [73] L. De Vittori, A. Gopakumar, A. Gupta, P. Jetzer, Gravitational waves from spinning compact binaries in hyperbolic orbits, Phys. Rev. D 90, 124066 (2014).
- [74] D. Bini, A. Geralico and J. Vines, Hyperbolic scattering of spinning particles by a Kerr black hole, Phys. Rev. D 96, 084044 (2017).
- [75] J. M. Bardeen, Proc. GR5, Tbilisi USSR, 174 (1968).
- [76] E. Ayón-Beato and A. García, The Bardeen Model as a Nonlinear Magnetic Monopole, Phys. Lett. B 493, 149 (2000).
- [77] S. A. Hayward, Formation and evaporation of nonsingular black holes, Phys. Rev. Lett. 96, 031103 (2006).

- [78] Z-Y Fan and X. Wang, Construction of Regular Black Holes in General Relativity, Phys. Rev. D 94, 124027 (2016).
- [79] B. Toshmatov, Z. Stuchlík and B. Ahmedov, Generic rotating black holes in general relativity coupled to nonlinear electrodynamics, Phys. Rev. D 95, 084037 (2017).
- [80] K. A. Bronnikov, Comment on "Construction of regular black holes in general relativity", Phys. Rev. D 96, 128501 (2017).
- [81] M. E. Rodrigues and E. L. B. Junior, Comment on "Generic rotating regular black holes in general relativity coupled to non-linear electrodynamics", Phys. Rev. D 96, 128502 (2017).
- [82] B. Toshmatov, Z. Stuchlík and B. Ahmedov, Note on the character of the generic rotating charged regular black holes in general relativity coupled to nonlinear electrodynamics, (2017). [arXiv:1712.04763]
- [83] D. Bini, A. Geralico and R. T. Jantzen, Gyroscope precession along general timelike geodesics in a Kerr black hole spacetime, Phys. Rev. D 95, 124022 (2017).
- [84] D. Bini and A. Geralico, Gravitational self-force corrections to tidal invariants for spinning particles on circular orbits in a Schwarzschild spacetime, Phys. Rev. D 98, 084021 (2018).
- [85] L. F. O. Costa, C. Herdeiro, J. Natário and M. Zilhão,

- Mathisson's helical motions for a spinning particle: Are they unphysical?, Phys. Rev. D 85, 024001 (2012).
- [86] L. F. O. Costa, J. Natário, Center of mass, spin supplementary conditions, and the momentum of spinning particles, Fund. Theor. Phys. 179, 215 (2015).
- [87] L. F. O. Costa, J. Natário, M. Zilhão, Spacetime dynamics of spinning particles exact electromagnetic analogies, Phys. Rev. D 93, 104006 (2016).
- [88] L. F. O. Costa, G. Lukes-Gerakopoulos, O. Semerák, Spinning particles in general relativity: Momentumvelocity relation for the Mathisson-Pirani spin condition, Phys. Rev. D 97, 084023 (2018).
- [89] K. P. Tod and F. de Felice, Spinning Test Particles in the Field of a Black Hole, Il Nouvo Cimento, 34, 365 (1976).
- [90] R. Hojman and S. Hojman, Spinning charged test particles in a Kerr-Newman background, Phys. Rev. D 15, 2724 (1977).
- [91] R. P. Kerr, Gravitational Field of a Spinning Mass as an Example of Algebraically Special Metrics, Phys. Rev. Lett. 11, 237 (1963).
- [92] J. M. Bardeen, P. W. H. Teukolsky, Rotating Black Holes: Locally Nonrotating Frames, Energy Extraction, and Scalar Synchrotron Radiation, Astrophys J. 178, 347 (1972).
- [93] O. Semerák, Stationary Frames in the Kerr field, Gen. Rel. Grav. 25, 1041 (1993).
- [94] E. P. Wigner, On Unitary Representations of the Inhomogeneous Lorentz Group, Annals. Math. 40, 149

- (1939) [Nucl. Phys. Proc. Suppl. 6, 9 (1989)].
- [95] D. Bini, A. Geralico and R. T. Jantzen, Black hole geodesic parallel transport and the Marck recipe for isolating cumulative precession effects, (2018) [Arxiv: 1807.10085].
- [96] C. W. Misner, K. S. Thorne and J. A. Wheeler, Gravitation, W. H. Freeman and Company, San Francisco (1973).
- [97] J. L. Synge, Relativity of the general theory, North-Holland Publishing Company, Amsterdam (1960).
- [98] H. S. Ruse, The potential of an electron in a spacetime of constant curvature, Quart. J. Math. 1, 146 (1930).
- [99] P. Gunther, Ein Beispiel einer nichttrivialen Huygensschen differentialgleichung mit vier unabhängigen Variablen, Arch. Rat. Mech. Analys. 18, 103 (1965).
- [100] H. A. Buchdahl, Characteristic function of Robertson Walker spaces, Gen. Rel. Grav. 3, 35 (1972).
- [101] H. A. Buchdahl and N. P. Warner, On the world function of the Godel metric, J. Phys. A 13, 509 (1980).
- [102] R. W. John, On the calculation of the geodetic distance and associated invariants relativistic gravitational fields, Ann. Phys. Leipzig 41, 67 (1984).
- [103] R. W. John, Trans. Inst. Phys. Estonian Acad Sci. 65, 58 (1989).
- [104] M. D. Roberts, The World Function in Robertson Walker Spacetime, Astrophys. Lett. Comm. 28, 349 (1993).